NOAA Technical Memorandum ERL WPL-21

MICROCOMPUTER-CONTROLLED ACOUSTIC ECHO SOUNDER

Edward J. Owens

Wave Propagation Laboratory
Boulder, Colorado
April 1977

noaa NATIONAL OCEANIC AND ATMOSPHERIC ADMINISTRATION / Environmental Research Laboratories

NOAA Technical Memorandum ERL WPL-21

MICROCOMPUTER-CONTROLLED ACOUSTIC ECHO SOUNDER

Edward J. Owens
Atmospheric Acoustics Program

Wave Propagation Laboratory
Boulder, Colorado
April 1977

UNITED STATES
DEPARTMENT OF COMMERCE
Juanita M. Kreps, Secretary

NATIONAL OCEANIC AND
ATMOSPHERIC ADMINISTRATION
Robert M. White, Administrator

Environmental Research
Laboratories
Wilmot N. Hess, Director

The NOAA Environmental Research Laboratories do not approve, recommend, or endorse any proprietary product or proprietary material mentioned in this publication. No reference shall be made to the NOAA Environmental Research Laboratories, or to this publication furnished by the NOAA Environmental Research Laboratories, in any advertising or sales promotion which would indicate or imply that the NOAA Environmental Research Laboratories approve, recommend, or endorse any proprietary product or proprietary material mentioned herein, or which has as its purpose an intent to cause directly or indirectly the advertised product to be used or purchased because of this NOAA Environmental Research Laboratories publication.

CONTENTS

CONTENTS (continued)

ACKNOWLEDGMENTS

The author wishes to express his sincere appreciation to Professor John A. Kleppe, Chairman of the thesis committee and research advisor, for his valuable guidance throughout this work. I especially want to thank Dr. C. G. Little, Director of Wave Propagation Laboratory (WPL), National Oceanic and Atmospheric Administration (NOAA), for his moral and financial support.

Appreciation is also extended to Dr. Freeman F. Hall, Jr., Chief, Atmospheric Acoustics Program in WPL, for his financial support and for allowing me the opportunity to complete this project.

ABSTRACT

This thesis is the result of research into new concepts of remote sensing of the atmosphere and includes a literature survey of the theory and practical application of atmospheric sounding using acoustic methods. The "state of the art" has been advanced in that a new type of system was designed, fabricated, and tested using modern digital methods. The major advances of replacing the typically troublesome facsimile recorder with a dot-matrix line printer using special characters called "tonels" and the development of a new and novel method of digital Doppler signal processing using a real covariance technique, is presented in detail.

The echosonde is capable of monitoring and displaying in real time the temperature fluctuations, turbulent velocity inhomogeneities, and vertical wind profile of the planetary boundary layer to a height of 680 meters and includes a microcomputer, a high-speed line printer, and various author-designed and -constructed digital and analog circuits.

User control of various system parameters and a wide choice of display possibilities make this a versatile and desirable atmospheric research tool.

MICROCOMPUTER-CONTROLLED ACOUSTIC ECHO SOUNDER

Edward J. Owens

NOAA/ERL/Wave Propagation Laboratory
Boulder, Colorado 80302

1. INTRODUCTION

The Earth, as viewed from space, appears as an oblate spheroid enveloped in a shell of transparent gases called the atmosphere. Half of this air mass is concentrated in a 6-km layer in which most of the clouds and weather are found — although air density, sufficient to measure, extends to a height of one thousand kilometers and more. The planetary boundary layer consists of the lowest one thousand meters where the atmosphere is the most dense and exhibits many curious vertical and horizontal distribution conundrums. Analysis of these phenomena requires a basic understanding of gravitation and consideration of the complex energy transformations continually taking place on this rotating globe.

Theories to explain the structure and motion of the atmosphere have been advanced by researchers using Newton's fundamental laws of motion and gravitation and the many branches of physics including thermodynamics. Remote and in-situ sensing of the atmosphere's structure and properties has long been a way of proving and expanding these theories. With the application of modern technology, remote sensing by means of acoustic echo sounding has proved to be an effective way of monitoring in great detail the larger scale features of the planetary boundary layer (Beran et al., 1973; Ottersten et al., 1973; Mandics and Owens, 1975).

Acoustic echo sounders or "echosondes" are used to monitor atmospheric temperature fluctuations by measuring backscattered echoes from acoustic tone bursts (Beran et al., 1971; Simmons et al., 1971; Hall, 1971; Wyckoff et al., 1973; Tombach et al., 1973; Brown and Keeler, 1974; Neff, 1975; and Mandics et al., 1975).

The basic components required for acoustic echo sounding are illustrated in Figure 1.1 and include a transmitting system to illuminate the turbulent region with acoustic energy and a sensitive receiving system to detect the scattered energy. The transmitting and receiving systems can share a common antenna (monostatic operation), or two spaced antennas can be used (bistatic operation). The scatter theory discussed in Chapter 2 shows that in the monostatic case echoes are obtained only from regions containing temperature inhomogeneities; in the bistatic case, echoes would be obtained from both mechanical turbulence and any temperature fluctuations present in the intersection volume of the two antenna beams.

The acoustic frequency used is very important, i.e., it is desirable to use as high an audio frequency as practicable, in order to ob-

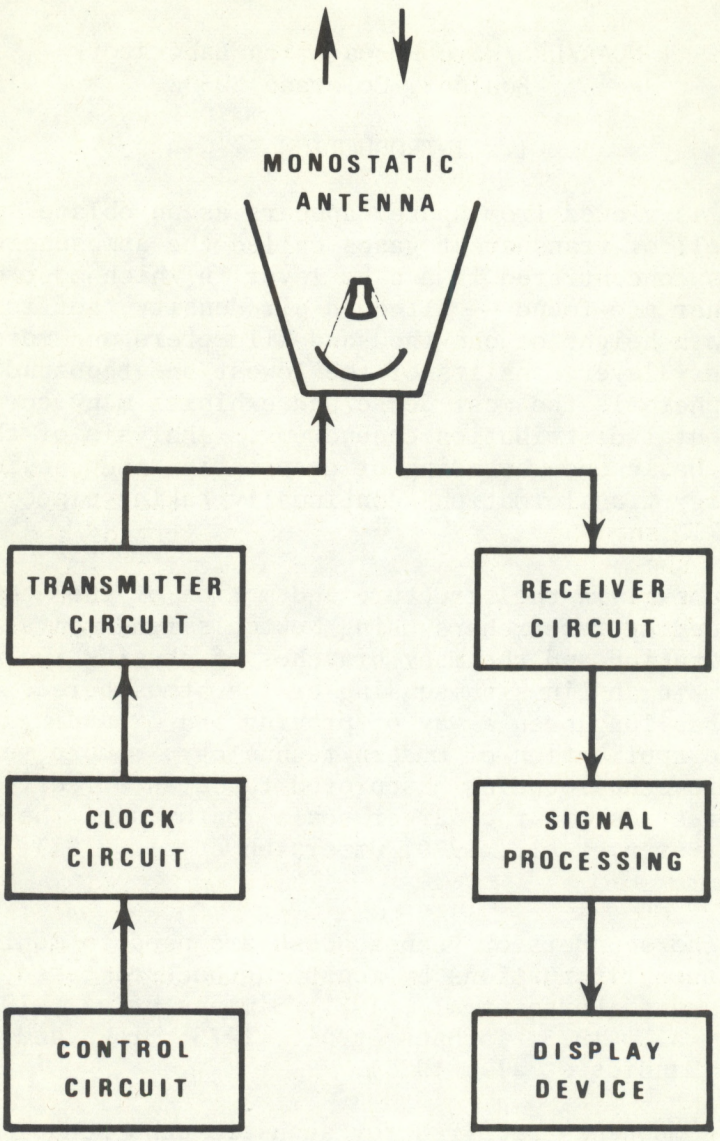

Fig. 1.1 Basic echosonde block diagram.

tain maximum angular resolution for a given antenna size and reduce the ambient acoustic background noise level. On the other hand, the rapid increase of acoustic absorption with frequency, makes the higher audio frequencies impracticable except at very short ranges. For heights up to about 700 m, a frequency of 2000 Hz is optimum.

The antenna size is determined by a compromise between cost and size and at 2000 Hz, collecting areas of the order of 1.8 m^2 can be expected to give adequate sensitivity up to a range of about 700 m.

From the earliest days of atmospheric acoustic echo sounding, large returns from the turbulent, convective daytime atmosphere have been monitored (Gilman et al., 1946). With the introduction of facsimile recorders, capable of displaying the backscattered echo intensity as a function of height and time, it became apparent that much of this structure went unobserved (McAllister et al., 1969). A typical facsimile recording of the unstable atmosphere, where the darkness of the record is proportional to the intensity of the backscatter echo, is shown in Fig. 1.2. Both 2-hour records, taken at the South Pole during the summer of 1975, show the diversity and complexity of the temperature structure in the lower atmosphere. Figure 1.2(a) shows a uniform ground-based inversion extending to a height of about 80 m, while Figure 1.2(b) shows thermal plume activity extending to a height of 200 m and apparently modifying an elevated inversion appearing between 300 and 400 m.

Many researchers, who daily study and analyze these records, have become proficient at interpreting and explaining the physical phenomena taking place. The average untrained viewer, however, is usually unable to understand and relate these phenomena to his own research or application. It has become apparent that a quantitative evaluation, in real time, of echo intensity and its Doppler shift is needed. To be used effectively, this information should be evaluated, reduced, and displayed in a manner suitable for the individual user's specific needs.

It was thought that recently developed, commercially available high-speed dot-matrix impact line printers could be effectively used as a display device for an acoustic echo sounder. A product search was successfully conducted and the challenge of generating intensity plots on an already very versatile display instrument was undertaken.

With the advent of microcomputers, modern digital logic circuits, and new digital signal processing schemes, the measurement of the Doppler shift of the received signal with reference to the transmitted frequency has been successfully used to measure wind direction and speed to heights of 600 meters and more (Beran et al., 1974; Beran and Willmarth, 1971).

The design and construction of echosondes is well established in papers by Simmons et al. (1971); Parry and Sanders (1972); Owens (1974, 1975); and Hall and Wescott (1974) with the major achievements occurring in the past five years. Early systems typically used commercially avail-

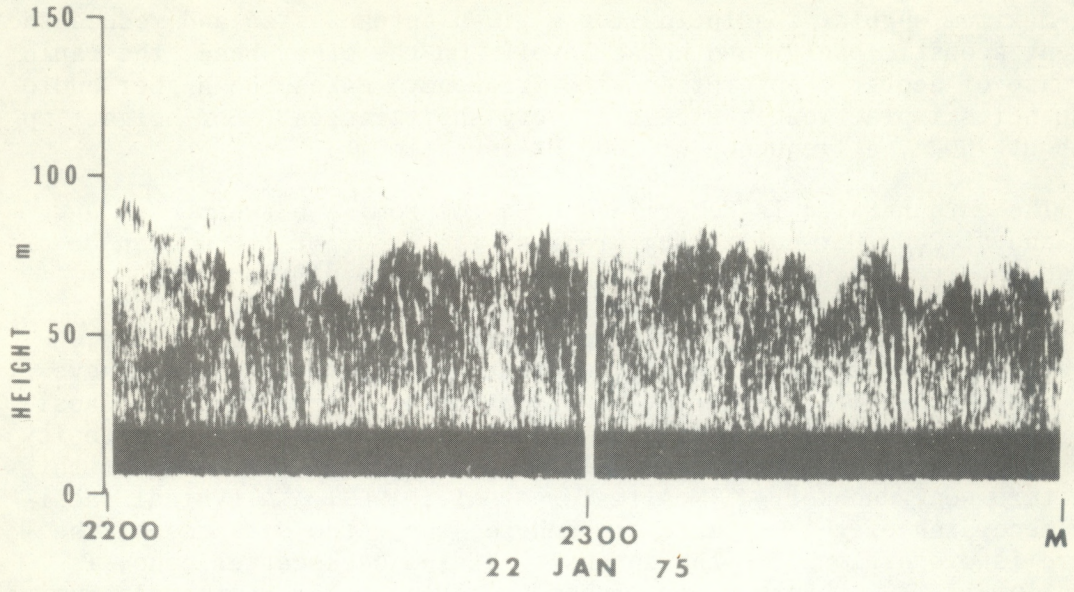

(a) Ground based inversion

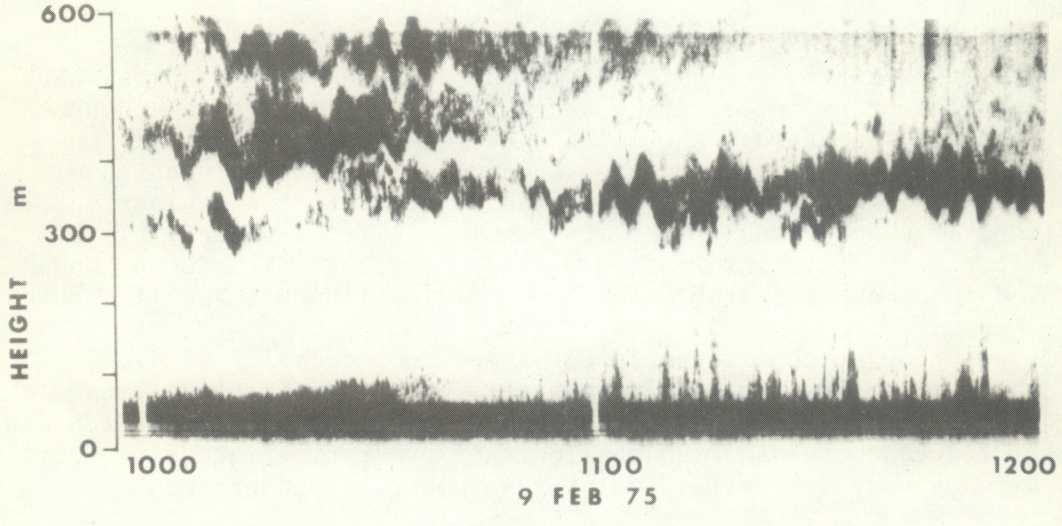

(b) Elevated inversion with plumes

Fig. 1.2 Typical echosonde facsimile records

able electronic equipment arranged to produce an analog version of a monostatic sounder. Facsimile recordings of the returned echo intensity presented a visual representation of the turbulent temperature structure, the height of thermal inversions and the presence of convective activity.

A second generation system evolved in 1972 interlacing some digital electronic circuits with the analog circuits, creating a smaller, portable, and less expensive system capable of a wide range of experimental uses (Owens, 1974). Recent advances in integrated circuit design, and especially the development of microcomputers, have opened a new dimension in electronic instrument design. Microcomputers are now applied to a variety of commercial and industrial uses where equipment control or monitoring and data processing are desired. It will be shown that this technology lends itself well to advancing the "state of the art" in echosonde design.

2. THEORETICAL CONSIDERATIONS

2.1 Echosonde Equation

Many excellent papers have been written formulating the echosonde equation. Acoustic energy is transmitted into the atmosphere and is scattered by any temperature fluctuations and/or turbulent velocity inhomogeneities present. The attenuated back-scattered energy is collected, amplified, and processed by the monostatic system to reveal information such as the stability of the planetary boundary layer, height of ground based and elevated inversions, height and cross sectional area of thermal plumes, and the presence of other convective activity.

The monostatic echosonde equation relates the range-compensated transducer voltage and frequency to the corresponding atmospheric inhomogeneities (Neff, 1975) and is written in the form (Kleppe, 1976):

$$P_r = P_t \frac{c\tau AG\sigma(r,f)L}{2r^2}$$

where

P_r = received power (watts)

P_t = transmitted power (watts)

A = collecting area of receiving antenna (m^2)

τ = tone burst duration (sec)

L = an attenuation factor including transmit and receive transducer efficiencies, atmospheric attenuation, and antenna efficiency

c = speed of sound (m/s)

r = range to target volume (m)

G = antenna gain

$\sigma(r,f)$ = scattering cross section per unit volume, i.e., fraction of incident power backscattered per unit distance into unit solid angle at frequency F.

Acoustic energy, in the form of longitudinal pressure waves, is attenuated by the atmosphere as a function of frequency, i.e., the higher the transmitted frequency the greater the attenuation. The sound level intensity at some distance from a source is given by

$$I = I_o e^{-kd}$$

where I_o is the source intensity, k is an attenuation term, and d is the distance. k is composed of three independent components, i.e.,

$$k = k_c + k_m + k_s$$

where k_c is the classical attenuation caused by the finite viscosity of air that leads to heating of the atmosphere as the sound wave passes, and by radiation and heat conduction from the high pressure regions of the sound wave, and is a function of the frequency squared, i.e.,

$$k_c = 4.24\ f^2 \times 10^{-11} m^{-1}.$$

k_m is molecular absorption caused by the transfer of energy from oxygen molecules vibrated by the sound wave to water vapor molecules. The energy transferred to the water vapor molecules is then radiated away in the form of heat and is a function of humidity and ambient air temperature. Molecular absorption decreases with temperature and is usually many times greater than the classical attenuation. This is why k_c is usually neglected.

k_s is excess attenuation caused by the scattering of energy by the atmospheric inhomogeneities themselves and is most often negligible.

2.2 Cross Section Interpretation

Chadwick and Little (1973) express the acoustic backscatter cross section per unit volume $\sigma(\theta)$, (see Fig. 2.1) as

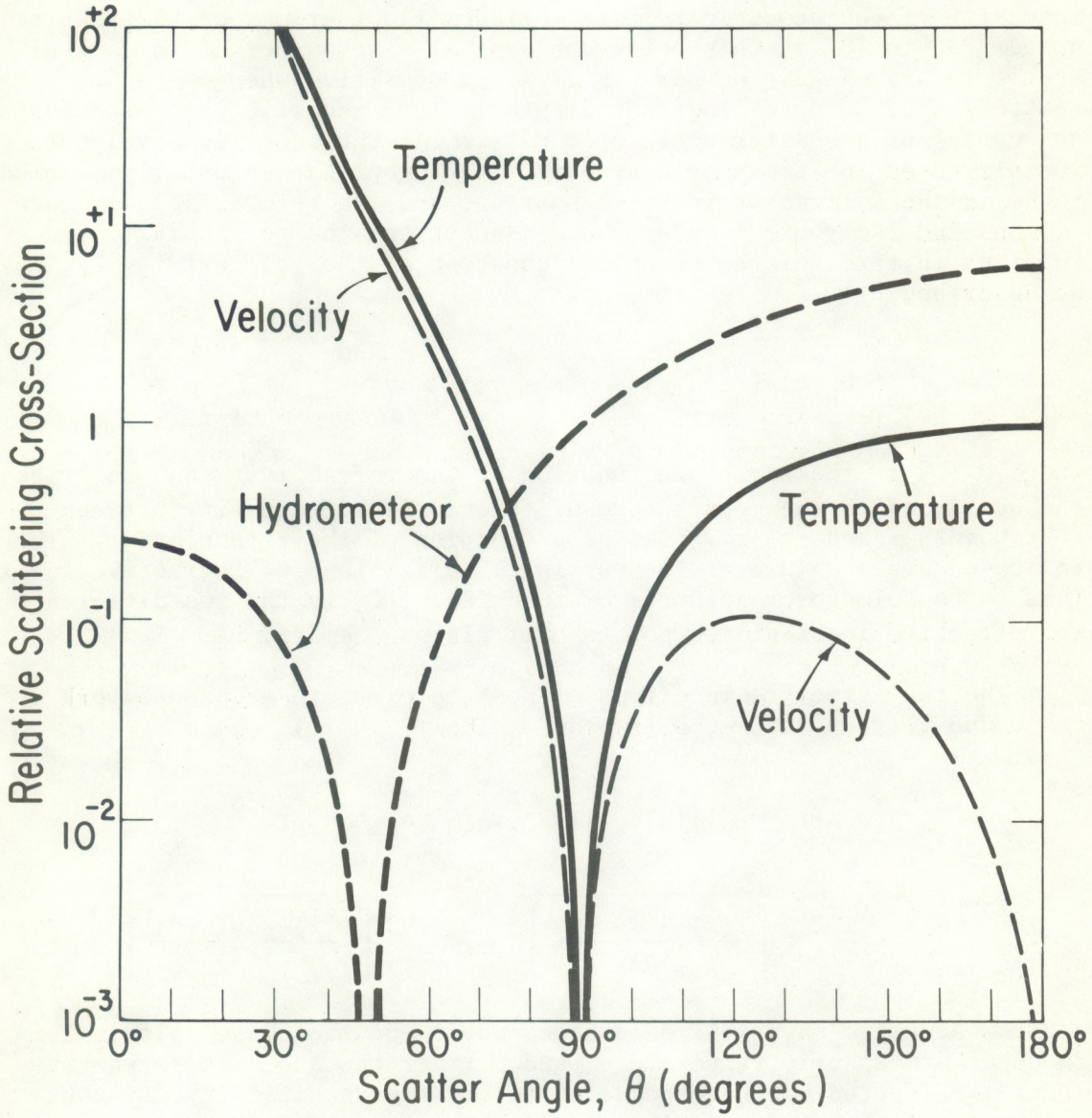

Fig. 2.1 Cross section scattering diagram

$$\sigma(\theta) = 2\pi k^4 \cos^2\theta \, \phi[2k \sin(\theta/2)]$$

where $4\pi\sigma(\theta)$ is the scattering cross section for acoustic waves as a function of scatter angle θ. The term $\phi[2k \sin(\theta/2)]$ is the spectral intensity of the acoustic refractive index fluctuations at the spatial number $2k \sin(\theta/2)$, this being the spatial wave number at which a bistatic radar, of wave number $k = 2\pi/\lambda$, is sensitive when operating at a scatter angle θ. The longitudinally polarized acoustic wave produces no scatter at a scatter angle of $\theta = \pi/2$. At the acoustic wavelength normally used in atmospheric studies, the turbulence is usually assumed to be in the Kolmogorov inertial subrange and, therefore, locally homogeneous and isotropic. Under these assumptions the refractivity fluctuations in terms of the structure constant of the refractivity C_n, can be described by

$$D_n(r) = \langle |n(x) - n(x + r)|^2 \rangle_{av} = C_n^2 \, r^{2/3}$$

where $D_n(r)$ is the structure function of the refractivity and describes the way in which the mean square difference in refractivity between two test points x and x + r varies as a function of their spacing, r. The indicated average is over the possible realizations of refractive index. Thus for a Kolmogorov spectrum of turbulence, C_n is the rms difference in refractive index at two points unit distance apart.

The two structure functions of most interest in echosonde work are those due to temperature, $D_T(r)$, and velocity, $D_V(r)$, where

$$D_T(r) = \langle |T(x) - T(x + r)|^2 \rangle_{av} = C_T^2 r^{2/3}$$

or

$$C_T^2 = \left[\frac{\overline{T(x) - T(x+r)}}{r^{1/3}} \right]^2 , \quad C_v^2 = \left[\frac{\overline{u(x) - u(x+r)}}{r^{1/3}} \right]^2$$

and for acoustic waves there is a dependence of the phase velocity of sound on atmospheric temperature, and further the acoustic refractive index is affected by the wind velocity or more specifically, by the component of the wind velocity along the acoustic ray path.

The formulae for the scattering cross sections in the inertial subrange of the Kolmogorov spectrum of temperature and velocity fluctuations can then be combined in the form:

$$\sigma(\theta) = 0.38 \, k^{1/3} \cos^2\theta [\sin(\theta/2)]^{-11/3} M^2$$

where

$$M = \left[\frac{C_v^2}{c^2} \cos^2 (\theta/2)^{0.13} + \frac{C_T^2}{T^2} \right]$$

and

$$k = 2\pi/\lambda \quad .$$

It is assumed that, on the spatial scale $[2k \sin (\theta/2)]^{-1}$, the velocity and temperature fields are uncorrelated and that the total scattered power is therefore the sum of the power scattered from the separate refractive index fluctuation fields.

The equations describing the scattering cross sections lead to a number of interesting points as discussed in the literature:

(a) The scattered acoustic power is only a weak function of acoustic wavelength, i.e., proportional to $\lambda^{-1/3}$, and the scattering is much stronger in the forward direction than in the back direction, i.e., proportional to $\sin(\theta/2)^{-11/3}$.

(b) Only temperature fluctuations contribute to backscatter power at $\theta = \pi = 180°$, and there is no scattering at all at $\theta = \pi/2 = 90°$.

(c) Uniform temperature gradients may also contribute to the scattered power (Hall, 1972).

A recent paper by Neff (1975) provides a comprehensive summary and discussion of the quantitative evaluation of acoustic echoes from the planetary boundary layer.

There are two basic parameters of interest to derive from echosonde data, that is, information contained in intensity as well as that in the Doppler spectrum. A serendipitous by-product of the returned echo signal is its frequency content.

2.3 Acoustic Doppler Information

One can analyze the frequency content of the returned signal and compare it with the transmitted frequency. The velocity of the air parcels along the acoustic beam can be derived.

Let f_t denote the frequency of the transmitted signal and assume that this signal is incident upon a target moving with a velocity $\vec{V}$ relative to the echosonde. The returned signal has a frequency, f_r, given by

$$f_r = f_t \left[\frac{1 + \frac{V_d}{c}}{1 - \frac{V_d}{c}} \right]$$

where V_d = radial velocity of the target
and c = speed of sound.

If we denote the unit vector directed inwards toward the echosonde as $\hat{r}$, then

$$V_d = \vec{V} \cdot r = |\vec{V}| \; |\hat{r}| \cos\theta$$

where θ is the angle between $\vec{V}$ and $\hat{r}$ and

$$f_r = \frac{f_t \left(1 + \frac{V_d}{c}\right)\left(1 + \frac{V_d}{c}\right)}{\left(1 - \frac{V_d}{c}\right)\left(1 + \frac{V_d}{c}\right)} = \frac{f_t \left(1 + \frac{2V_c}{c} + \frac{V_d^2}{c^2}\right)}{1 - \frac{V_d^2}{c^2}} \; .$$

In the usual case the Doppler shift is much less than the speed of sound or $\frac{V_c}{c} << 1$ which is nearly always true for vertical velocities in the atmosphere, and certainly for those velocities measured under normal convective plume conditions. It follows then that:

$$f_r \approx f_t \left(1 + \frac{2V_d}{c}\right) = f_t + \frac{2V_d}{\lambda}$$

where $\lambda = c/f_t$ the wavelength of the transmitted frequency. The Doppler shift f_d is then determined to be

$$f_d = f_r - f_t = \frac{2V_d}{\lambda} \; .$$

The Doppler frequency f_d carries a sign so that Doppler velocities toward the echosonde are positive and those away from the echosonde are negative.

For an assemblage of scatterers moving with different velocities the returned signal will contain components corresponding to all the Doppler velocities, giving in general a spectrum of Doppler frequencies according to the number and relative strengths of the scatterers moving with each velocity.

A profile of the vertical component of wind using a single vertically pointing, pulsed monostatic system can be measured by selecting gates at successive distances along the antenna beam.

A bistatic system can also be used to measure wind velocity. Consider the system configuration shown in Figure 2.3. The Doppler velocity component is taken along the direction of the vector $(\vec{K}_s - \vec{K}_o)$ which is the bisector of the angle formed between the directions from the scatterers to the transmitter and to the receiver. The magnitude of the wind resolved along the vector $(\vec{K}_s - \vec{K}_o)$ is then given as V cos B. The Doppler shift is then

$$f_d = \frac{2V_d}{c} f_t \cos(\alpha).$$

Since

$$\cos(\alpha) = \cos(90° - \frac{\theta}{2}) = \sin(\frac{\theta}{2})$$

and

$$V_d = V \cos(B),$$

then

$$f_d = \frac{2V}{c} f_t \sin(\frac{\theta}{2}) \cos(B).$$

The monostatic system provides measurements of C_T as well as radial Doppler measurement of wind velocity. For horizontal wind the axis of the monostatic system must be tilted. Generally either two or three receivers (sharing the same transmitter) are employed to measure the entire wind vector. This development assumes that refraction or bending of the beams is negligible. A more detailed account of the Doppler equation is given by Beran and Clifford (1972), Georges and Clifford (1972), and Brown (1972).

Interpretation of echosonde data to separate the effects of mean wind, mechanical turbulence, and temperature fluctuations depends on the solution of the equations for the propagation and scattering of a sound pulse in a moving refractive field as presented by Brown (1972).

Acoustic echoes from a moving scattering volume, such as an acoustic pulse propagating through a wind shear for example, may be considered as having a narrow-band, time-varying spectrum. The analysis of this information can provide estimates of several meteorological parameters of interest. The mean of the spectrum for example, is related to the mean wind in the scattering volume and the variance related to the turbulence within the same scattering volume.

Beran (1971) points out that the much lower speed of acoustic waves (as compared with electromagnetic waves) can introduce some errors into the acoustic Doppler measurements. He further points out that the method of obtaining acoustic spectra differs from radar because of the

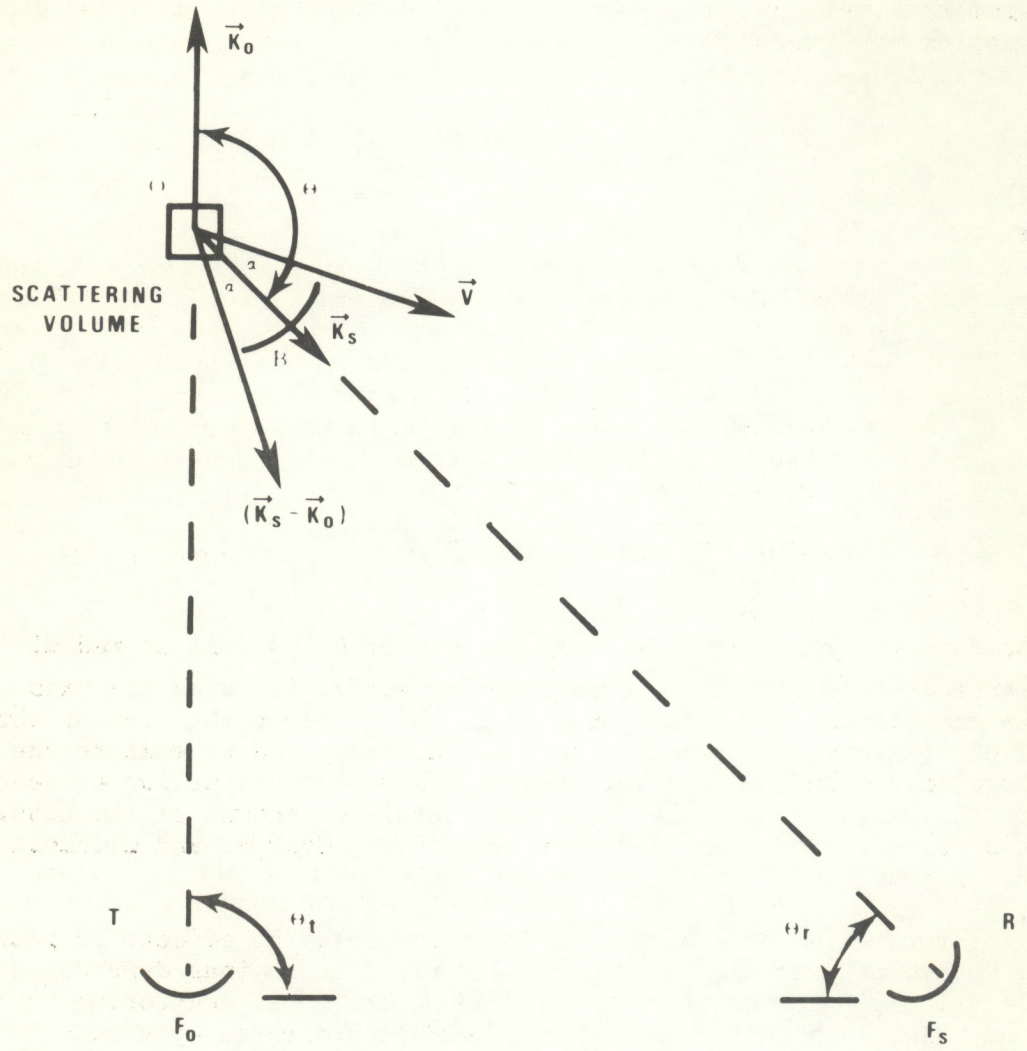

Fig. 2.3 Schematic diagram showing the orientation of wave vectors from a transmitter, T, and a receiver, R. The vector $(K_s - K_0)$ represents the Doppler shift produced by a wind V.

much higher PRF in electromagnetic radar. The final spectrum generated from a radar return is extracted from information contained in each of many separate pulses and it is this spectrum that is used to reproduce the Doppler frequency; in the acoustic case, a spectrum can be generated for each pulse. The higher pulse repetition rate of the radar does not increase the accuracy if the signal-to-noise ratios and overall duty cycles (fraction of time that the transmitter is on) are equal in the two cases. An improvement can be made by averaging the acoustic spectra from succeeding pulses, although this reduces the horizontal resolution by increasing the size of the total volume being considered. This is due primarily to the ambient air motion during the time required to collect the sample.

Quantitative interpretation of the received signal Doppler spectrum requires detailed analysis of the echosonde equations. Individual scatterers of varying reflectivity and moving at different turbulent velocities are distributed throughout the volume defined by the antenna beams and the pulse length in space. Recent theoretical studies of Doppler shifted echosonde data by Brown and Clifford at the Wave Propagation Lab, NOAA, Boulder, Colorado (WPL) have focused on the acoustic Doppler radar equation and its solutions.

The need remains for advanced study of signal processing techniques in order to select efficient real time methods for the analysis and display of echosonde data. A few of the possible methods for signal analysis are discussed in the following sections with particular emphasis on the correlation techniques.

2.4 Signal Processing Methods for Echosonde Data

Interest in the application of digital methods to signal processing has rapidly increased and numerous approaches to digital signal processing have been proposed. The major concern today is to select a method that minimizes the required number of computations and storage requirements. As noted earlier, the method for obtaining spectra for echosonde data differs from radar primarily because of the much higher radar PRF. In the acoustic case a spectrum can be generated for each pulse. For a given signal-to-noise and duty cycle an increased PRF does not improve the accuracy of the estimate; however, some improvement results in averaging acoustic spectra from succeeding pulses with a resulting loss of horizontal resolution.

The input data to the echosonde signal processor will be assumed to consist of analog variations representing signal plus noise (or noise alone) corresponding to a given time or range extent.

For many applications the complete Doppler spectrum is not needed, so only the mean velocity (or some suitable central value) and its velocity spread are recorded. This greatly simplifies data handling by avoiding the problems attendant to the measurement and storage of complete spectral information. Moreover, the accuracy attainable in

measurements of the mean Doppler velocity and velocity spread is generally greater than that in complete spectral measurements, although the same general constraints apply to the required length of record. The deviation must be long compared with the decorrelation time but short compared with the time scale or target variability. The time constants or integration times for measurements of the mean velocity and velocity spread should be determined for echosondes. The signal can generally be modeled as "locally" stationary since in such cases the range gates can be chosen such that the time trends are very slow relative to the instantaneous fluctuations of the data.

The first moment of the spectrum is called the mean Doppler velocity and is denoted by $\bar{v}$. The second moment about the mean Doppler velocity is called the Doppler variance and is denoted by σ_v^2. The mean of the spectrum $\bar{v}$ is related to the mean wind in the scattering volume and the variance σ_v^2 is related to the turbulence within the same scattering volume.

The following paragraphs will present theoretical considerations for correlating alternate methods of processing Doppler radar information. These techniques are studied for possible applications to echosonde data. They are similar to the "pulse pair" estimation theory which offers a new potential for Doppler signal processing. They permit the economic implementation of a real-time signal processor and as such reduce the large amounts of data normally produced by a Doppler echosonde to a manageable level.

2.5 Spectral Mean and Variance Estimation Using Digital Methods

The process of digitizing consists of converting continuous data into discrete numbers. It is important to have a sufficient number of samples to describe properly the significant information in the high frequencies. On the other hand, sampling at points that are too close together will yield correlated and highly redundant data, and increase greatly the labor and cost of calculations. To cut down the number of samples, one should decrease the sampling rate to the lowest rate that will avoid aliasing errors. One should choose the sampling interval $h = \Delta t$ such that

$$h = \frac{1}{2f_c}$$

where $\frac{1}{f_c}$ is the smallest "period" in record. The h chosen must be small enough so that aliasing will not be a problem. Although the cut-off frequency f_c (Nyquist frequency) is a theoretical requirement, more points or less sample interval is usually recommended in practice for improved results. For accurate correlation function measurements where the correlation function has frequencies near f_c, one should choose

$h = \frac{1}{4f_c}$. If power spectra measurements are the prime consideration, then choosing $h = \frac{2}{5f_c}$ should be sufficient.

The maximum number of correlation lags, m, can be chosen such that

$$m = \frac{1}{Bh}$$

where

B = desired equivalent resolution bandwidth for power spectra calculations.

The sample size N can be selected such that

$$N = \frac{m}{\varepsilon^2}$$

where

ε = normalized standard error described for spectral calculations.

The associated minimum record length, T_r is then

$$T_r = Nh.$$

A more detailed account of these parameters is given by Sirmans and Doviak (1973).

The calculation of autocorrelation functions is of most interest here. For N data values x(n), n = 1,2,...,N from a transformed record x(t) that is stationary with zero mean, the estimated autocorrelation function at the displacement rh can be written in the form:

$$\hat{R}_x(rh) = \frac{1}{N-r} \sum_{n=1}^{N-r} x_n x_{n+r} \qquad r = 0,1,2,\ldots,m$$

where

r = lag number,

m = maximum lag number,

and $\hat{R}_x$ = estimate of true autocorrelation function.

Since the quantity m represents the maximum number of correlation lag values, the maximum displacement is

$$\tau_{max} = mh.$$

As a "rule of thumb", it is desirable to keep the maximum lag m about one-tenth the sample size N. This will tend to avoid certain instabilities that can occur in autocorrelation function estimates.

A "raw" estimate, $\hat{G}_x(f)$, of a true power spectral density function can be defined for an arbitrary f in the range $0 \leq f \leq f_c$ by

$$\hat{G}_x(f) = 2h\left[\hat{R}_o + 2\sum_{r=1}^{m-1}\hat{R}_r \cos\left(\frac{\pi rf}{f_c}\right) + \frac{rf}{f_c} + \hat{R}_m \cos\left(\frac{\pi mf}{f_c}\right)\right] \quad (1)$$

where

h = time interval between samples

$\hat{R}_r$ = estimate of the autocorrelation function at lag r

m = maximum lag number

f_c = cutoff frequency = $\frac{1}{2h}$.

The function $\hat{G}_x(f)$ is often called a "periodogram."
The values of the function $\hat{G}_x(f)$ can be calculated only at the m + 1 special discrete frequencies where

$$f = \frac{kf_c}{m} \qquad k = 0,1,2,\ldots,m.$$

This will provide $\frac{m}{2}$ independent spectral estimates since spectral estimates at points less than $\frac{2f_c}{m}$ apart will be correlated. At these discrete frequency points:

$$\hat{G}_k = \hat{G}_x\left(\frac{kf_c}{m}\right) = 2h\left[\hat{R}_o + 2\sum_{r=1}^{m-1}\hat{R}_r \cos\left(\frac{\pi rk}{m}\right) + (-1)^k \hat{R}_m\right]. \quad (2)$$

The index k is called the harmonic number, and $\hat{G}_k$ is the "raw" estimate of the power spectral density function at harmonic R, corresponding to the frequency $f = \frac{kf_c}{m}$.

A final "smooth" estimate of the power spectral density may be found by using "Hanning" (Blackman and Tukey, 1958).

Let $\tilde{G}_k$ represent the "smooth" estimate at harmonic k, where the ~ replaces the ^. Then at the m+1 frequencies

$$f = \frac{kf_c}{m} \qquad k = 0,1,2,\ldots,m \qquad \text{one obtains}$$

$$\begin{aligned}
\tilde{G}_o &= 0.5\hat{G}_o + 0.5\hat{G}_1 && k = 1,2,\ldots,m-1 \\
\tilde{G}_k &= 0.25\hat{G}_{k-1} + 0.5\hat{G}_k + 0.25\hat{G}_{k+1} && \qquad (3) \\
\tilde{G}_m &= 0.5\hat{G}_{m-1} + 0.5\hat{G}_m \ .
\end{aligned}$$

Smoothing is usually necessary since the periodogram (raw estimate) equation (1) is an inefficient estimate of the true spectral density. The variability of these estimates does not decrease with increased record length or sample size. This leads to the requirement of smoothing the periodogram or, equivalently, weighting the correlation function nonuniformly.

An alternate equivalent way to obtain equation (3) is in terms of a Hanning lag window weighting function D_r defined by

$$\begin{aligned}
D_r &= D(rh) = 1/2\ (1 + \cos\frac{\pi r}{m}) && r = 0,1,2,\ldots,m \\
D_r &= 0 && r > m.
\end{aligned} \qquad (4)$$

Note that $D_o = 1$ and $D_m = 0$. Equation (4) may now be combined with equation (2) to yield a condensed formula for the smooth estimates at harmonics k = 0,1,2,...,m. Specifically,

$$\tilde{G}_k = \tilde{G}_x\left(\frac{kf_c}{m}\right) = 2h\left[\hat{R}_o + 2\sum_{r=1}^{m-1} D_r\hat{R}_r \cos\left(\frac{\pi rk}{m}\right)\right].$$

An alternate conventional spectrum estimate can be computed directly from the discrete Fourier transform of the windowed data

$$\hat{X}(\omega) = \sum_{k=0}^{N-1} x(k)\ W(k)\ \varepsilon^{jwk} \qquad 0 \leq \omega \leq \pi$$

and

$$\hat{G}_x(\omega) = |\hat{X}(\omega)|^2 .$$

It is usually necessary for accurate power spectrum estimates to implement some sort of averaging. For acoustic Doppler applications this can be done by choosing a suitable range gate over which the Doppler spectrum may be assumed stationary, by calculating a periodogram for several successive pulses, and finally by averaging these consecutive periodograms to obtain a more accurate power spectrum estimate. For a tilted monostatic Doppler echosonde a long enough period of time averaging will result in the removal of short term vertical motions of the atmosphere and the resulting spectrum will represent only Doppler information due to the mean horizontal wind.

A common disadvantage of these conventional methods is the time and expense required to compute the spectrum estimates. An improved method for spectrum estimation has been recently proposed (Keeler and Griffiths, 1976). This technique uses an adaptive linear prediction filter that updates its coefficients as each new sample is received. A least mean square gradient adaption algorithm is employed to adapt the filter coefficients. These continuously updated coefficients are then used to compute a simplified linear prediction spectrum for the input sequence. The simple modification of the standard linear prediction spectrum consists of removing the gain calculation; it has the effect of producing a spectral estimate that is unaffected by changes in the input signal strength and depends solely on the spectral width of the input signal spectrum. Thus the resulting adaptive linear prediction spectrum can not only track changes in the mean frequency of the received spectrum but can also track changes in the width of the Doppler spectrum.

The theory of the adaptive linear prediction method (ADAP) is covered in detail by Keeler and Griffiths (1976). In general terms the mathematical basis of the technique may be understood from the following discussion.

The basic form of the classical linear prediction filter, G, is shown in Figure 2.5.1 where z^{-1} denotes a one-sample delay in the z transform domain. The one-step prediction of the input sequence x(k) is formed as a linear combination of L previous input values. Thus

$$\hat{x}(k) = \sum_{\ell=1}^{L} g_\ell x(k-\ell)$$

where g_ℓ is the ℓ^{th} coefficient of the prediction filter. An error sequence is formed from the actual x(k) by

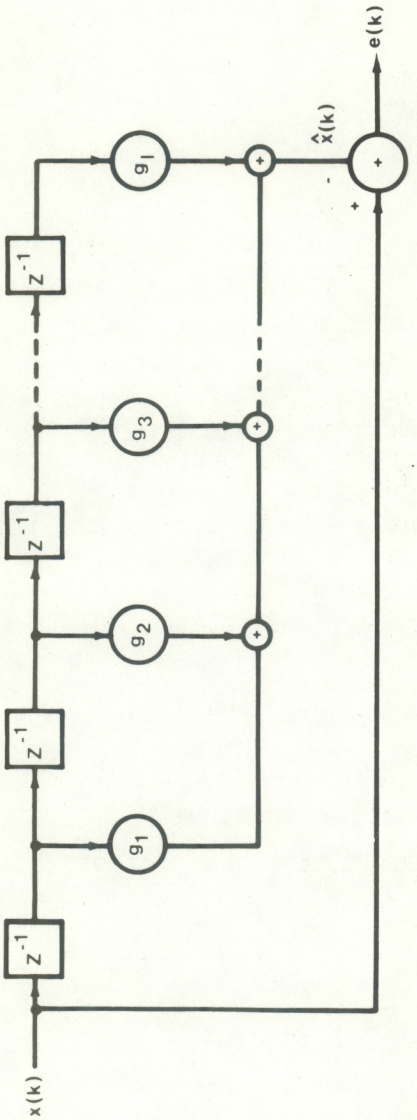

Fig. 2.5.1 Basic linear prediction filter.

$$\varepsilon(k) = x(k) - \hat{x}(k).$$

The filter coefficients, G^*, which produce the minimum mean square error (mmse) may be expressed in matrix form as

$$G^* = R_{xx}^{-1} P_x$$

where

$$G^{*T} = [g_1^*, g_2^*, \ldots\ldots, g_L^*]$$

$$P_x^T = [r_x(1), r_x(2), \ldots, r_x(L)]$$

$$R_{xx} = \begin{bmatrix} r_x(0) & r_x(1) & \ldots\ldots & r_x(L-1) \\ r_x(1) & & & \cdot \\ \cdot & & & \cdot \\ \cdot & & & \cdot \\ r_x(L-1) & \ldots\ldots\ldots & & r_x(0) \end{bmatrix}$$

where T denotes the transpose and $r_x(1)$ represents the autocorrelation function.

The linear prediction spectrum $M_x(\omega)$ can be expressed in terms of the optimum prediction filter coefficients as

$$M_x(\omega) = \frac{r_x(0) - \sum_{\ell=1}^{L} g_\ell^* r_x(1)}{\left|1 - \sum_{\ell=1}^{L} g_\ell^* e^{-jw\ell}\right|^2} .$$

When the filter coefficients have their optimum value, G^*, the numerator of

$$M_x(\omega) = \frac{E[\varepsilon^2(k)]_{min}}{\left|1 - \sum_{\ell=1}^{L} g_\ell^* c^{-jwT}\right|^2} .$$

The finite impulse response mmse whitening filter has a transfer function given by

$$H'(\omega) = \frac{1 - \sum_{\ell=1}^{L} g_\ell^* e^{-j\omega\ell}}{E|\varepsilon^2(k)|_{min}^{1/2}} \quad .$$

Therefore, the linear prediction spectrum estimate, $M_x(\omega)$, is identical to the inverse of the magnitude squared transfer function of the optional whitening filter, $H'(\omega)$, or

$$M_x(\omega) = \frac{1}{|H'(\omega)|^2} \quad .$$

The function of a whitening filter is to produce a white sequence from a colored input sequence. Using z transform notation,

$$H(z) = \sum_{k=0}^{\infty} h(k) z^{-k} \quad ,$$

the input sequence to the whitening filter, x(k), may be generated from a white sequence w(k) modified by a coloring filter s(z) as shown in Figure 2.5.2. The linear prediction filter must contain sufficient zeros to cancel the poles of s(z) used to color the original white sequence.

A modified linear prediction spectrum estimate, $Q_x(\omega)$, is used in the ADAP method where

$$Q_x(\omega) = \frac{1}{|H(z)|^2} = \frac{1}{\left|1 - \sum_{\ell=1}^{L} g_\ell^* c^{-j\omega\ell}\right|^2}$$

with the difference being the gain factor, $E[\varepsilon^2(k)]$. The ADAP method is an alternate method for obtaining the prediction filter coefficients for the filter structure shown in Figure 2.5.3. The method is a time domain iterative technique which avoids the two-step procedure of first computing the autocorrelation values and then solving the normal equations. The method is described by Keeler and Griffith (1976).

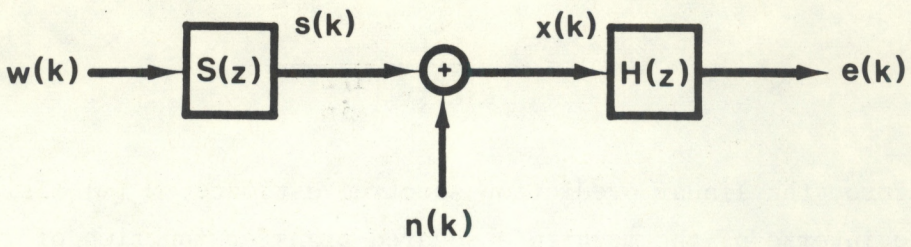

Fig. 2.5.2 Generation of input sequence and whitening filter.

2.6 Real Correlation (RC) Approach to Spectral Moment Estimation

MATHEMATICALLY, the problem is to determine the statistics of certain functions of the estimators of the spectral density of a random process.

The autocorrelation function $R(\tau)$ for a real stationary process $x(t)$ is defined as:

$$R(\tau) = \lim_{T\to\infty} \frac{1}{T} \int_0^T x(t)\, x(t+\tau)dt.$$

The quantity $R(\tau)$ is always a real valued even function with a maximum at $\tau = 0$. It may be either positive or negative.

For a sampled signal of N data values $x(n)$, $n = 1,2,\ldots,N$ from a record $x(t)$ which is stationary with zero mean, the estimated autocorrelation function at the displacement $\tau = rT$ is defined by the formula

$$\hat{R}_x(rT) = \frac{1}{N-r} \sum_{n=1}^{N-r} x(n) \quad x(n+r) \qquad r = 0,1,2,\ldots,\tau_{max}$$

where

n = maximum lag number,

N = sample record length,

and $\tau_{max} = mT$.

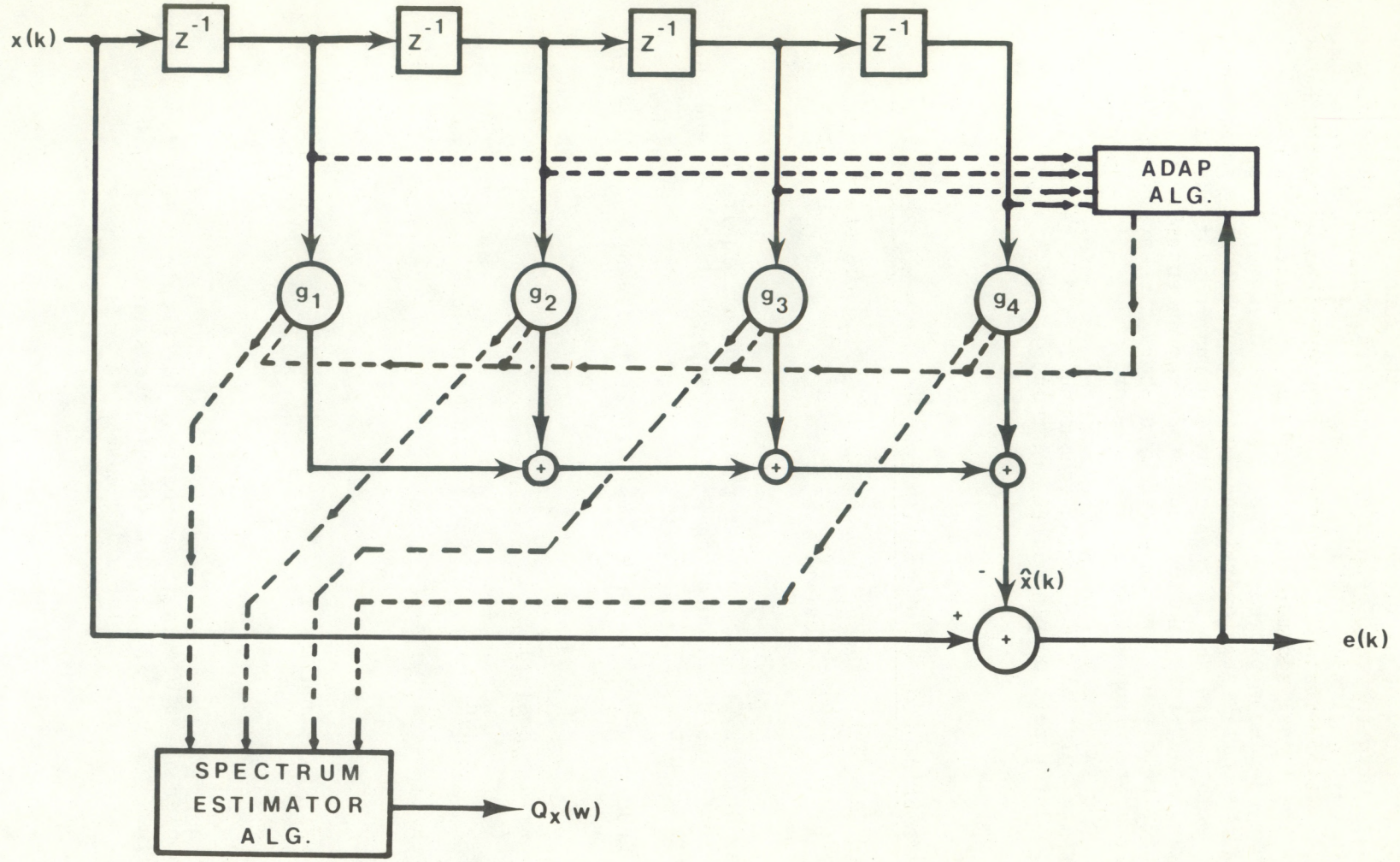

Fig. 2.5.3 Basic adaptive linear prediction spectrum estimator.

For cases involving Doppler echosonde data the function $R(\tau)$ persists periodically with the same period as the underlying sine wave. Because of turbulence the signal $x(t)$ is not a pure sinusoid but is rather composed of a set of sine waves whose mean frequency changes with the motion of the signal scatterers. The signal is therefore a nonstationary narrowband random process. The echosonde data may however be considered as "locally" stationary since in such a case the time trends are very slow relative to the instantaneous fluctuations of the data. The time-varying power spectrum then computed from an ensemble of sample records will be closely approximated by a short time-averaged power spectrum computed from a single sample record.

A typical plot of $R(\tau)$ for an echosonde record is shown in Figure 2.6.1 for zero Doppler shift, that is,

$$w = w_o$$

The function $R(\tau)$ has the general form

$$R(\tau) = e^{-\alpha|\tau|} \cos(w\tau).$$

For echosonde data it appears that the value of α is quite small. This has been confirmed by calculating $R(\tau)$ for several data runs and observing the results.

The model of $R(\tau)$ over the first few cycles is given with $\alpha = 0$,

$$R(\tau) \approx \cos(w\tau)$$

for values $w = (2n + 1)\frac{\pi}{2}$

$$R(\tau) = \cos(w\tau) = 0$$

and for

$$w_o = \frac{\pi}{2} \text{ and } \tau = 1$$

$$R(1) = 0.$$

When a Doppler shift occurs it is possible to calculate $R(\tau)$ for each of the values $\tau = 0,1,3,5,\ldots$ and compare the sign of $R(\tau)$ with that calculated for a zero Doppler shift case.

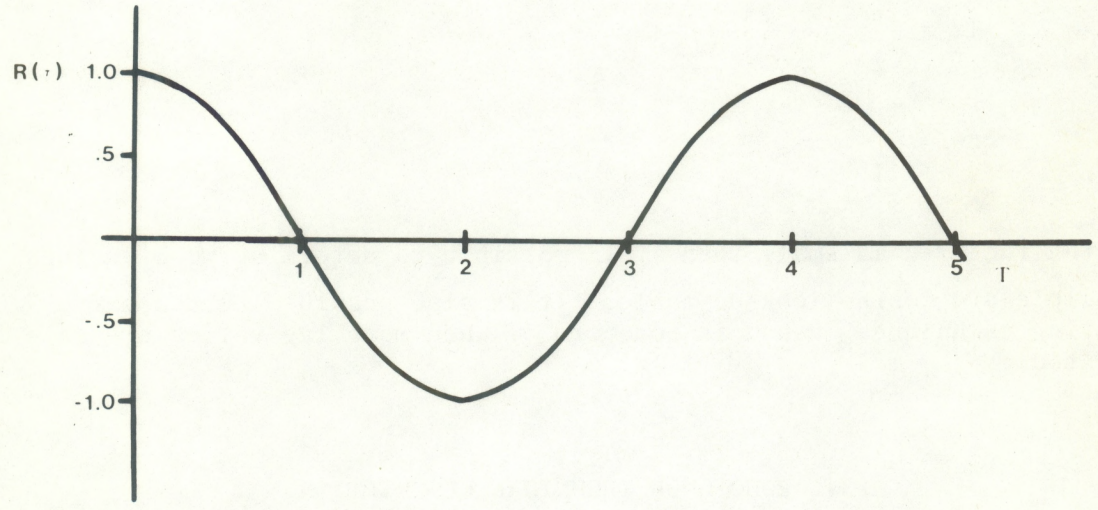

Fig. 2.6.1 Plot of R(τ) with zero Doppler shift.

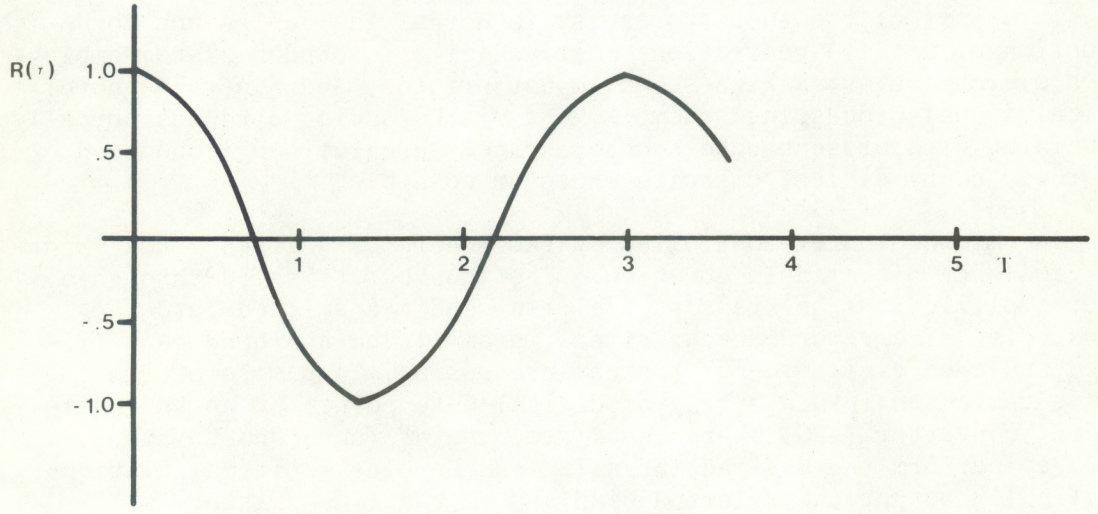

Fig. 2.6.2 Plot of R(τ) with non-zero Doppler shift.

Figure 2.6.2 shows a case where the Doppler shift

$$w_1 > w_o$$

and R(1) is negative. For this case

$$T_1 = \frac{2\pi}{w_1} = \frac{2\pi}{w_o + \Delta w} < 4$$

$$\Delta w = \frac{2\pi}{T_1} - w_o.$$

If the factor α is small then it is possible to determine w_1 by using a simple arc cosine look-up table. It is also possible to use curve-fitting techniques when α is not zero or when more lag values are calculated.

3. ECHOSONDE TECHNICAL DESCRIPTION

3.1 General Description

This part of the thesis presents in detail the design and construction of a third-generation, mostly digital, sounder system employing a microcomputer, a high-speed impact printer, and a new and novel digital signal-processing scheme. Most of the analog circuits normally associated with present echo sounder systems are refined, condensed, and replaced by digital circuits wherever possible.

The microcomputer controlled system generates a fixed 2-kHz transmit frequency of variable duration. The tone burst is fed through a power amplifier to the transducer element and transmitted into the atmosphere. The returned echo signal is amplified and band-pass filtered and then available for further processing. A sample of the signal is converted into a string of digital data points by an analog-to-digital converter (ADC) where the microcomputer functions to store, average, perform the desired intensity and Doppler shift calculations, and finally output the selected displays to the line printer.

The echo intensity is obtained by a combination analog and digital circuit employing standard designs and components. The Doppler information is obtained by the implementation of a real covariance procedure whose design allows near real-time measurement of the radial wind component. Processing of the data needed to calculate wind and temperature profiles is performed with operator control of averaging time and types of displays. The incorporation of the microcomputer also allows the evaluation of many other meteorologically significant quantities such as thermal inversion height, plume size and speed, etc.

The output device used in this system is a special-character high-speed impact line printer used for displaying the desired output and for communicating with the microcomputer. A standard keyboard is integrated into the design to allow the operator to list and modify, if necessary, some of the variable parameters of the system. The replacement of the typically troublesome facsimile recorder by a line printer is most important to the design of the system. Not only does this eliminate the need for special paper, high voltage writing amplifier, pens, and alignment procedures, but it also eliminates the usual restrictions on what can be displayed in real time. Present facsimile-type recorders display only the time-range echo intensity whereas the line printer can display individual or many combinations of outputs, including echo intensity, temperature (C_T) contours and values, wind (C_V) profiles and values, and supporting meteorological data. The 132-column computer-type printout paper used in the line printer is less expensive and can last for several weeks of operation without replacement, depending on the outputs generated. Copies can be made in real time by using multi-layered paper, and replacement and storage represent no special problems.

The key to generating three-dimensional plots of time, range, and echo intensity (inherent with facsimile recorders) on two-dimensional paper lies in the special characters (defined here as "tonels") incorporated into the line printer. These tonels are a 4 x 6 matrix of dots divided into 10 quantizing levels by the unique arrangement of the dots. A zero level produces no dots and results in a blank space while the maximum intensity level contains 24 dots in a 4 x 6 array. Both the number of dots and their arrangement serve to form the quantizing levels that produce the third dimension (intensity) on the paper when integrated with the eyes. For example, a system is installed in the field programmed to transmit a 50-m-sec tone burst at 2 kHz. The receiver delay is set at 70 m-sec and the pulse repetition rate is 2 sec. The user has selected an output that displays the intensity plot on the line printer. The ground or zero altitude is at the left edge of the printout and the 100th column of the paper corresponds to an altitude of 340 m. The intensity of the returns quantized into 10 levels is displayed by using the special characters or tonels described above. After one hour of operating time the paper will have advanced 180 lines (about 16 inches), resulting in a conventional intensity display. The operating program then disables the tone burst for one minute and backs the paper up exactly the number of lines generated during the past hour. Contours of C_T and C_V are displayed in columns 101 through 132. Some external meteorological data can also be displayed. Since all of this information has been gathered, averaged, and calculated during the preceding one hour or longer period of time, it is readily available and quickly printed out. The time of day is then printed in the blank space generated by the hour marker. Finally, the bookkeeping routines in the operating program are performed and at the proper time the sequence is started again.

Note that various different plots or combinations of plots could have been selected. For instance, the intensity could have been plotted as usual and then C_T, C_V, etc. plotted on successive pages to be separated later. Another logical scheme is to plot the intensity record using the first 80 columns and printing values of C_T or C_V on the remaining 52 columns.

A unique and worthwhile characteristic of the microcomputer is its variety of memories. The selected and proven operating program is stored in Read-Only-Memory (ROM) on a separate 4 K x 16 word memory module. Once written and debugged, this "burned" program is foolproof and cannot be accidentally changed by the operator. Upon application of power to the system this program is read and executed without assistance from an operator. If many different non-volatile programs are required then several sets of inexpensive ROMs can be programmed and be simply replaced in sockets on the memory module.

For general research applications, however, an operating program allowing user input has been established. Upon initial activation of the program, several user responses are required with the system asking questions expecting either the default values or system changes to be made. The variable system parameters are listed along with their default values and printed out on the line printer for later reference. In some cases the various output displays are explained and user selection of one or more is made. Once the program has started, the system operates completely automatically and requires no further input or monitoring. The calculations are performed and the selected outputs generated. Intentional interruption of the program can be accomplished by pressing the BREAK key on the keyboard or by switching the system to the HALT mode by means of the HALT/RUN switch on the power supply chassis. Unintentional interruption of the program can be accomplished only by a complete power failure. Restoration and restart of the operating program, however, is accomplished automatically upon return of normal power supply voltages.

3.2 Theory of Operation

The theory of operation of the echosonde can be followed from the detailed schematic diagrams in Appendices A and B and from the block diagram in Figure 3.2.1. The Control Unit consists of 5 printed circuit boards (PCB's) in a 3-in by 11-in chassis mounted in an attractive 8 3/4-in by 17 1/2-in by 17-in relay rack mountable equipment case. A removable front panel and slide mounted equipment shelf allows easy access to the printed circuit boards and various electronic equipment for easy maintenance and calibration.

Figure 3.2.2 shows the arrangement of the 5 PCB's installed in a DEC H9270 backplane assembly. The pre-wired assembly rack provides mechanical integrity for the PCB's and also allows easy interconnection to the various control, power supply, and signal lines.

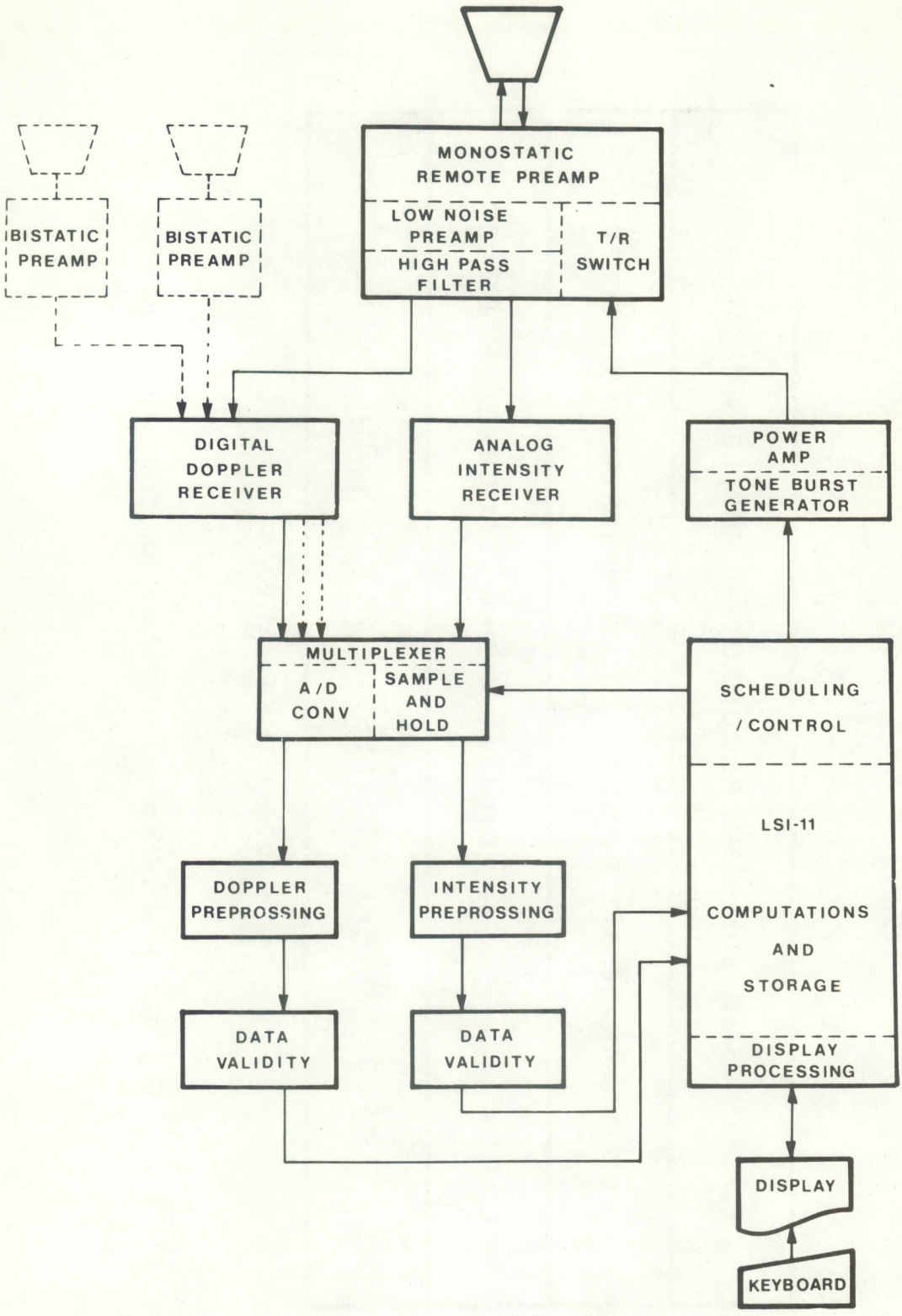

Fig. 3.2.1 Echosonde block diagram

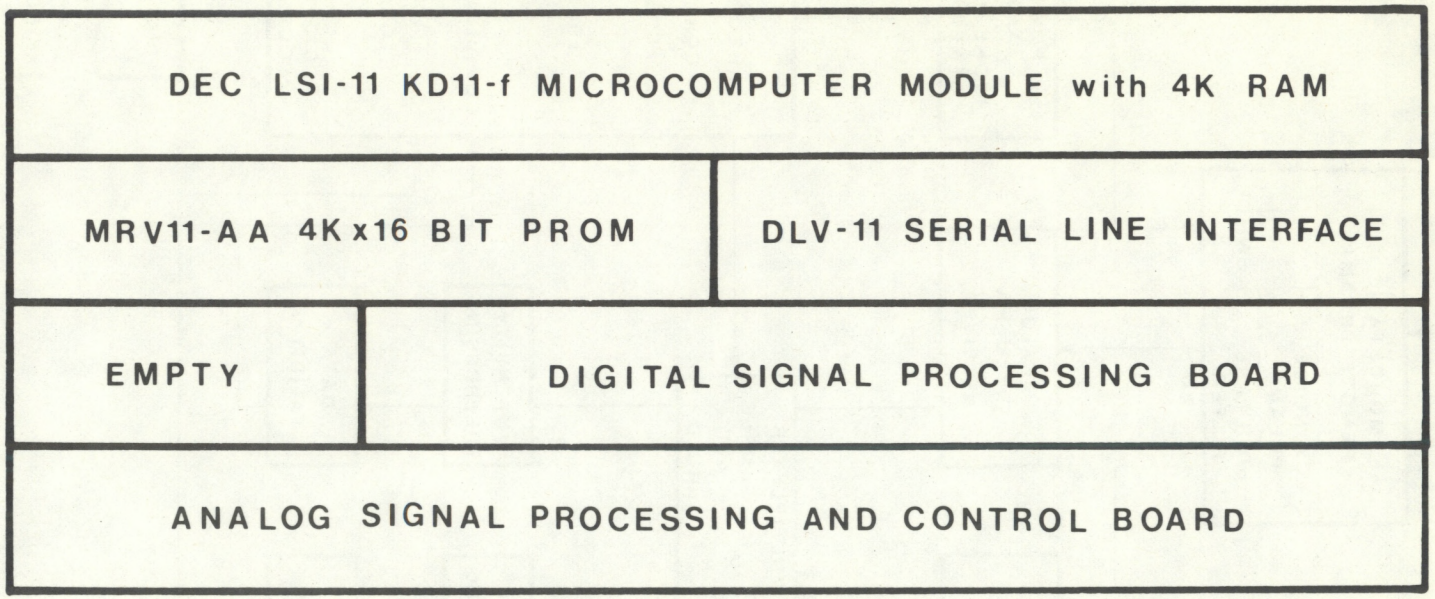

Fig. 3.2.2 Printed circuit board configuration.

Figure 3.2.3 shows in block diagram form the arrangement of the power supplies, power amplifier, and control unit. Various switches, lamps, fuses, etc. are mounted on the front panel and chassis.

The LSI-11 microcomputer (PCB1) is the basis for all computational and some control functions. It has been summarized in section 3.5 with references to complete and detailed descriptions in various publications. Included in the appendices for better understanding of the LSI system are the bus pin assignments, instruction sets, and the 7-bit ASCII code.

The serial interface board (PCB2) handles all serial I/O communication between the printer and the microprocessor. The unibus concept and special decode logic designed on the users printed circuit boards make possible communication between any boards and the terminal. This may indeed prove useful in succeeding versions of the echosonde as refinements and modifications are made.

The 4K dynamic PROM memory board (PCB3) stores the operating program(s) that analyze and display the data. The memory may consist of "burned" read-only memory (ROM), programmable read-only memory (PROM), random access memory (RAM) or combinations of the above. This board, in future systems, may be eliminated by replacing some of the resident 4K RAM on the CPU board with the "burned" ROM if the operating program and storage area required is small enough.

The Echosonde Control Board (PCB4) is the heart of the system and consists of the various analog and digital circuits needed to create a basic monostatic echosonde. These circuits include the following:

i) The clock circuit is the basis for all timing and transmit frequency generation. The output of a stable 200-kHz square-wave oscillator is counted down by various "count-down" circuits to yield the 20 kHz square-wave input to the transmitter circuit and the 1-kHz square-wave input to the gating circuits.

ii) The transmitter circuit further reduces the 20-kHz signal to a 2-kHz symmetric square-wave. A multiple feedback active band-pass filter shapes the transmit frequency which is then gated by the TRANSMIT GATE to form the transmitted tone burst. The tone burst is amplified and fed to the remote preamplifier automatic transmit-receive circuits through the long multi-conductor cable.

iii) The control gate circuits use the 1-kHz signal from the clock as a 1-msec timing base for the DIP-switch selectable TRANSMIT, RECEIVER-DELAY, and PULSE REPETITION RATE control gates, which in turn control the respective electronic switches and reset circuits.

iv) The HOUR MARKER circuit sends a control signal to the TRANSMIT GATE circuit to disable it, thus deactivating the transmitted tone burst, for 1 min every hour. This places a 1-min timing mark on the facsimile record which can be synced to a time-of-day clock. A moveable jumper

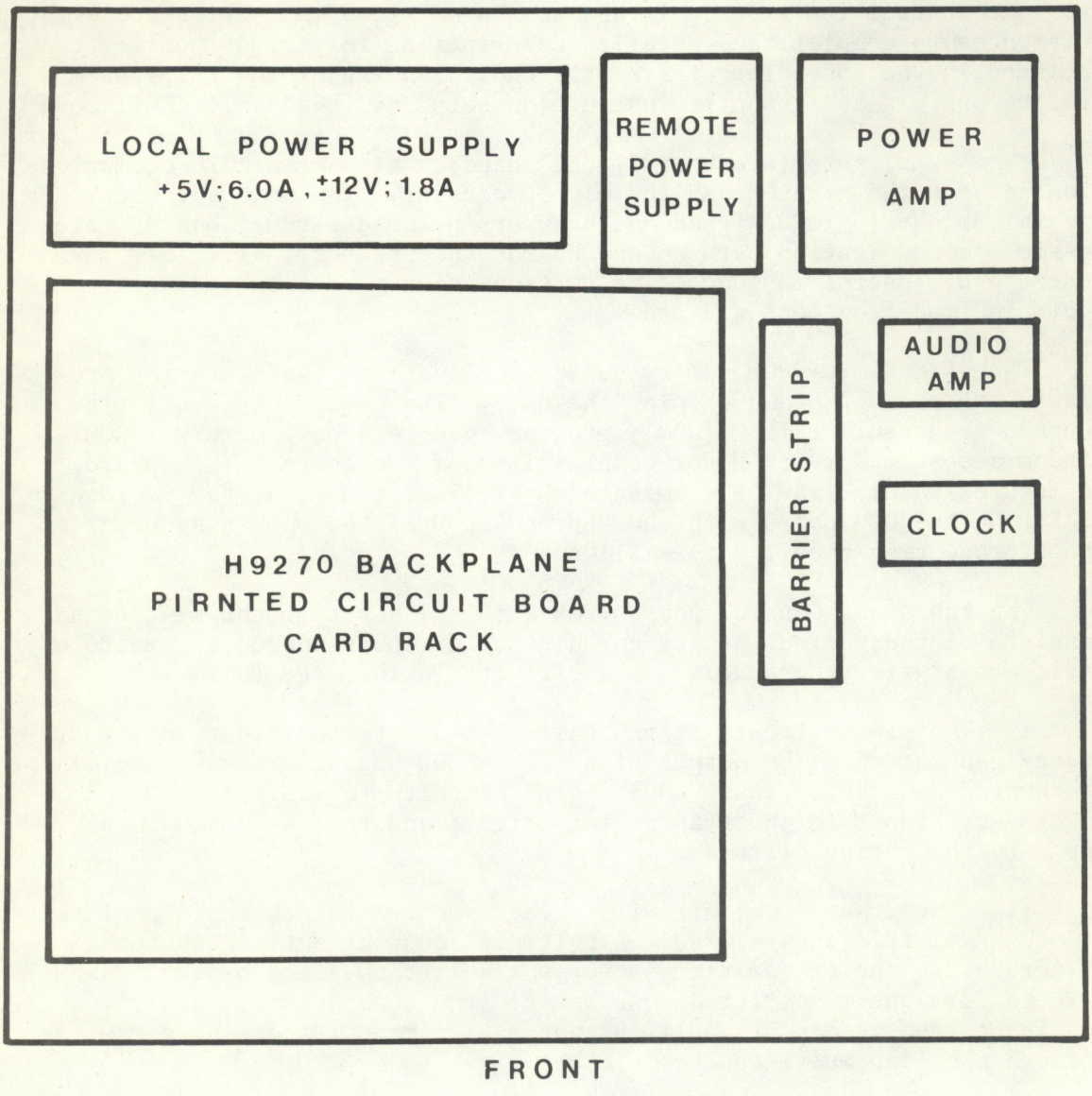

Fig. 3.2.3 Echosonde component block diagram.

on the PCB allows this circuit to be by-passed and transmitter tone bursts to continue indefinitely.

v) The receiver circuit uses the RECEIVER GATE control pulse to switch the output of the remote preamplifier, i.e., the wide-band raw echo signal, through a variable gain amplifier to the X input of an analog multiplier. A range-compensating gain ramp, generated by an 8-bit digital-to-analog converter and various frequency counting circuits, is fed to the Y input of the analog multiplier. The resulting signal is the gated range-compensated raw echo signal which is then band-pass filtered.

vi) The filter, a commercially available, very narrow, active band-pass filter, is tuned to the 2-kHz transmit frequency and has a band-width of ± 35 Hz.

vii) The detector, a BURR-BROWN true RMS-to-D.C. converter converts the relatively noise-free signal into a low frequency signal proportional to the square root of the received echo intensity. This signal is available for use by digital processing circuits located on the Digital Signal Board (PCB3).

The Digital Signal Board (PCB3) converts four channels of analog data into digital form for processing by the microcomputer. The four data signals are echo intensity and Doppler Signals 1, 2, and 3. In the basic monostatic system described herein, only two of these signals are used, i.e., the echo intensity and the monostatic Doppler signal. A complete three-channel Doppler wind sensing system is achievable with appropriate programming of the microcomputer.

The raw echo signal from the remote preamp is band limited by a simple 2-pole band-pass filter. The resultant signal is mixed by an X:Y multiplier with a local oscillator of frequency 1900 Hz. The signal is low-pass filtered and presented as one input to the multiplexer circuit. A standard sample and hold (S/H), buffer amplifier and 12-bit A/D converter follow and are all computer controlled. The output of the A/D converter is presented to the data-bus through specially designed interface logic circuits.

The Remote Preamplifier, located next to the antenna up to 200 ft from the control unit, acts as an automatic switch for transmit and receive modes, and amplifies the very weak echo signal. Several sections of high-pass filters eliminate the usually strong, low-frequency ambient background noise.

The remaining electronics consist of a triple output (+ 5 VDC, ± 12 VDC) power supply for the printed circuit boards, an isolated ± 15-VDC power supply for the electronic circuits located in the remote preamp, the 100-watt tone burst amplifier, and the audio monitor amplifier.

Space and power considerations for future modification have been incorporated into the basic design, including the possible addition of a digital cassette recorder. It was my goal to design a system that started with a simple monostatic sounder monitoring only echo intensity and that could be easily expanded to produce a three-channel wind-sensing system.

3.3 Microcomputer Description

3.3.1 General Description of LSI-11

The LSI-11 microcomputer system is configured by selecting various LSI-11 module options which are installed in a backplane (Fig. 3.3.1.1). This concept allows the individual system requirements to vary greatly while making efficient use of the microcomputer in a compact, flexible system design.

The LSI-11 system used in this echosonde includes the KD11-F microcomputer, an MSVII-B memory module, a DLV11 serial line unit interface module, A DRV11 general-purpose parallel line unit interface module, two general-purpose printed circuit boards, and the H9270 backplane assembly.

The KD11-F is a single 8.5-in by 10-in module that contains the LSI-11 microprocessor and a 4K- by 16-bit semiconductor read/write memory. Its features include: 1) direct addressing of up to 32K 16-bit words; 2) efficient processing of 8-bit characters without the need to rotate, swap, or mask; 3) asynchronous operation that allows the system components to run at their highest possible speed; 4) a hardware memory stack for handling structural data, subroutines, and interrupts; 5) direct memory access for high data rate devices; 6) eight general-purpose registers that are available for data storage, pointers, and accumulators; 7) fast interrupt response without device polling; 8) the entire PDP-11 instruction set of programming instructions; 9) a jumper-selected power-up mode that enables restart through a power-up vector, console OCTAL DEBUGGING TECHNIQUE (ODT) microcode subset, and a bootstrap program; and 10) on-board 4K RANDOM ACCESS MEMORY (RAM). The ODT microprogram controls all the manual entry/display functions through the serial ASCII device which is capable of transmitting and receiving ODT commands and data.

The MSV11-B is a 4K by 16-bit dynamic MOS read/write memory on an 8.5-in by 5-in module. Refresh is automatically performed by the KD11-F processor microcode under program control or by an external device.

The DLV11 is a serial line unit interface on an 8.5-in by 5-in module. User-changeable jumpers select the crystal-controlled baud rates (50-9600 band) and the serial word format, including the number of stop bits, number of data bits, and even, odd, or no parity bit.

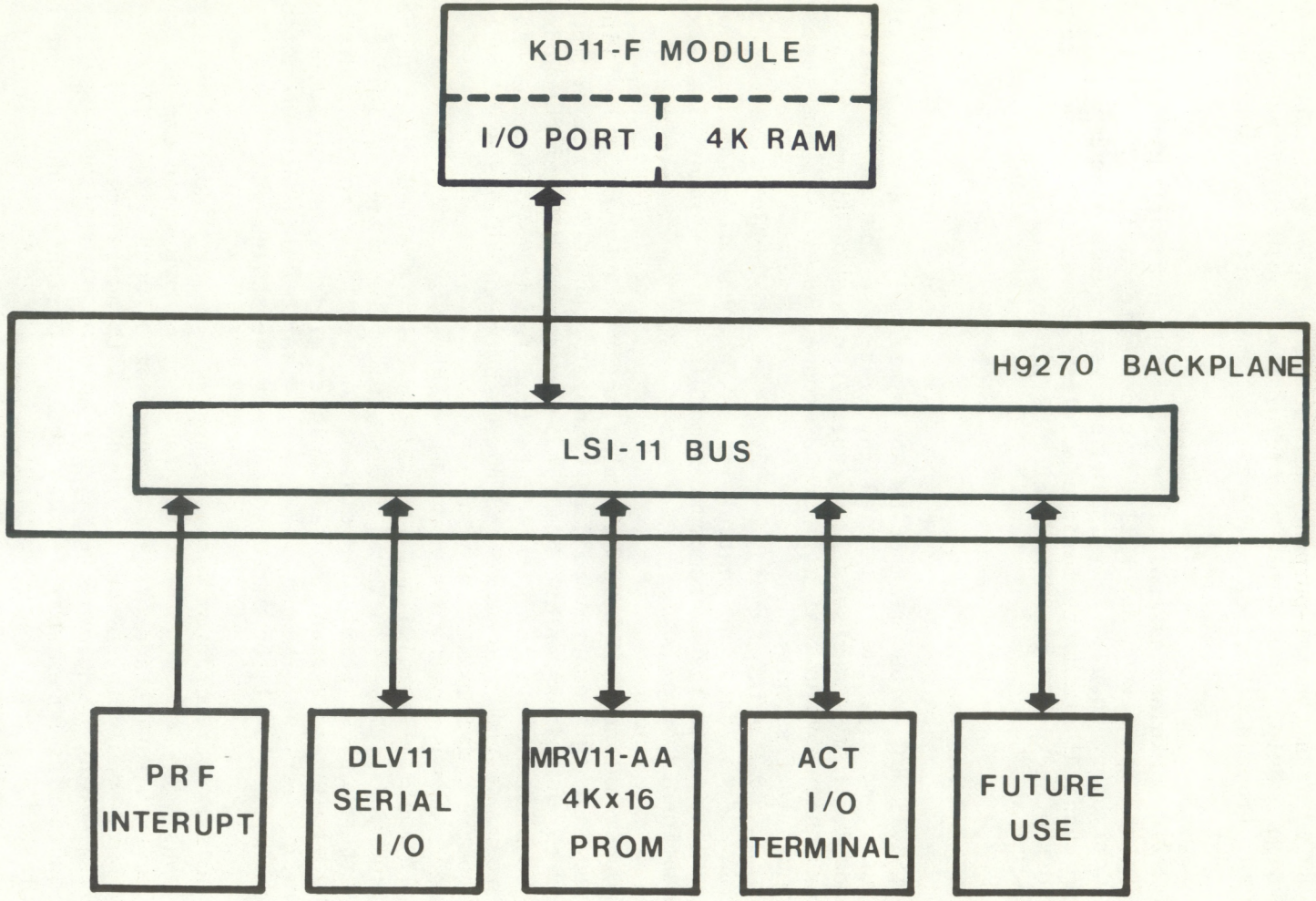

Fig. 3.3.1.1 LSI-11 System architecture.

The DLV11 can be connected to a 20-mA current loop peripheral device or to EIA-compatible devices (modems).

The DRV11 is a general-purpose parallel line unit interface on an 8.5-in x 5-in module. Two 40-pin connectors are included on the module for user interface application. These are the 16-bit input and the 16-bit output.

The H9270 backplane assembly is a prewired rack for the LSI-11 I/O bus pinning and can accept one KD11-F microcomputer and up to six LSI-11 interface or memory modules. It includes a card guide assembly that provides mechanical stability for the modules. Power and ground are applied to the backplane through a screw terminal block.

3.3.2 I/O Bus Structure

The LSI-11 I/O unibus is used as an interface between the LSI-11 microcomputer, memory, the peripheral interface and the user's special-purpose modules. It comprises 17 control lines and 16 address/data lines. The unibus concept means that all modules connected to this bus receive the same interface signals.

The 33 address/data and control lines are open-collector lines which are asserted low with the microcomputer module capable of driving six device locations.

Both address and data words are time multiplexed over 16 bus lines. For example, during a programmed data transfer, the LSI-11 microcomputer first asserts an address on the bus for a fixed time. After the address time has been completed, the actual data transfer is asynchronous and requires a response from the addressed device by means of bus synchronization and control signals.

The 17 control signal lines include two daisy-chained grant signals that provide a priority-structured I/O system. The highest priority device is the module electrically closest to the KD11-F module. Higher priority devices pass a grant signal to lower priority devices only when not requesting service. Memory modules or other modules that do not use these signals must still be wired to connect the chain.

The KD11-F microcomputer module contains a memory address register and a 4K bank address decoder for its resident memory which can be assigned to bank 0 with addresses ranging from 0000 to 3777. The MSV11-B memory module is assigned to bank 1 with addresses ranging from 4000 to 7777. Bank 7 addresses ranging from 28,000 to 31777 are normally used for addressing non-memory devices such as peripheral device interface modules.

The bus provides a vectored interrupt capability for the interface devices thus eliminating device polling required in interrupt processing routines. This results in quicker service times in systems where many devices require interrupt servicing. When a device receives an interrupt acknowledge, the KD11-F inputs the devices interrupt vector. The vector points to two addresses that contain a new processor status word (PSW) and the starting address of the interrupt service routine for the device. Bit 7 of the PSW when asserted denies any further interrupt grants until the present interrupt service routine is complete and has relinquished control. Immediately upon returning to the operating program a new PSW is assigned, again allowing already existing or future interrupts.

One bus signal line (BEVNT) functions as an external event interrupt to the KD11-F module. This signal line can be connected to a frequency source, such as a line frequency, and used as a line time clock (LTC) interrupt. Another bus signal line (BHALT-L) when asserted places the processor in the HALT mode allowing a peripheral device to invoke console ODT microcode operation.

Power-up/power-down sequencing is controlled by two bus signals (BPOK-H and BDCOK-H). BPOK-H in its true state implies that primary power is normal. BDCOK-H is in its true state when sufficient dc power is available (and voltages are normal) for normal system-logic operation. These signals are produced by the user's power supply system external to the LSI-11 system components.

3.3.3 LSI-11 System Operation

3.3.3.1 Bus Cycles

Each processor instruction requires one or more I/O operations, the first one being a data input transfer (DATI), which fetches an instruction from the location addressed by the program counter. This operation is called a DATI bus cycle. If no additional operands are referenced in memory or in an I/O device, no additional bus cycles are required for instruction execution. However, if memory or a device is referenced, additional DATI, data input/output (DATIO or DATIOB), or data output transfer (DATO or DATOB) bus cycles are required. Between these bus cycles, the processor can service DMA requests. In addition, the processor can service interrupt requests prior to an instruction fetch (DATI bus cycle) if the processor's priority is zero.

3.3.3.2 DMA Operations

DMA I/O operations involve a peripheral device and system memory by which the device can transfer data to or from the 4K memory on the processor module or any read/write memory module along the bus. Memory addressing, timing, and control signal generation/response have to be

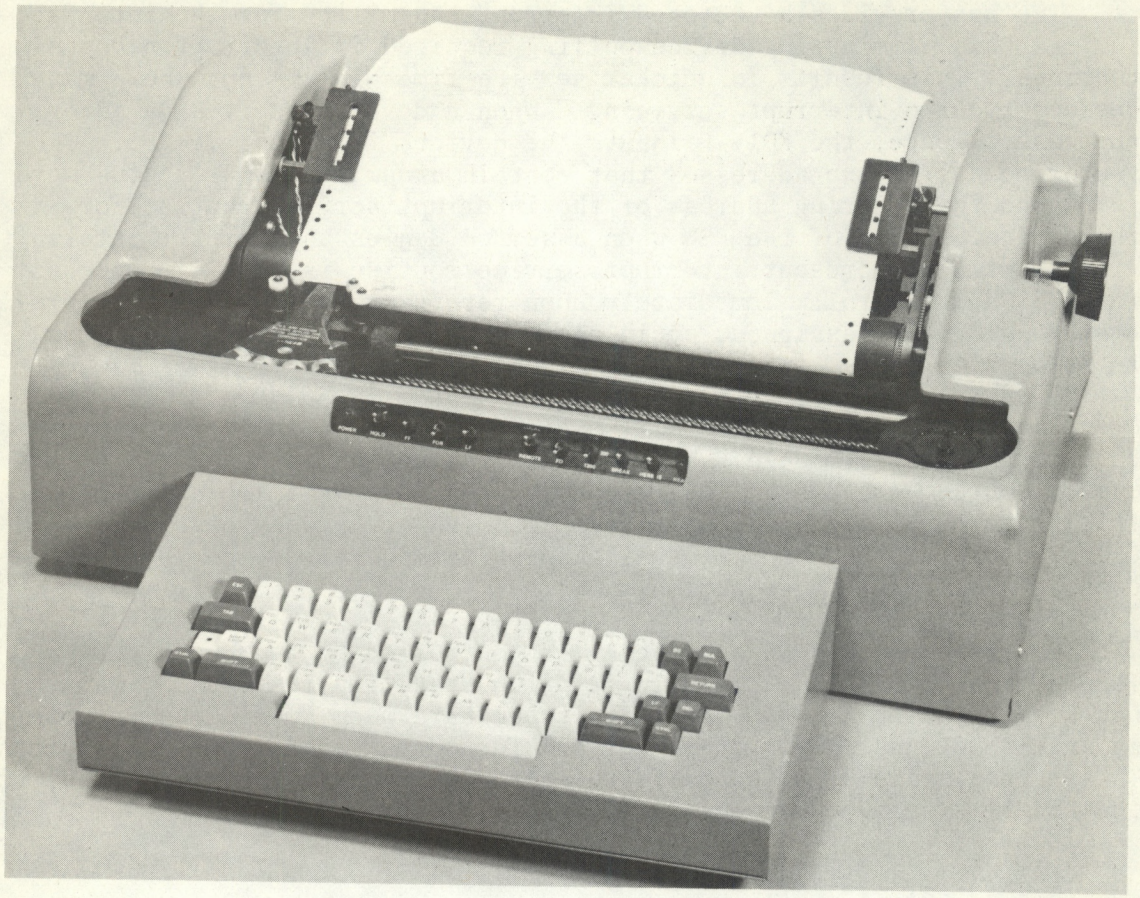

Fig. 3.4.1 ACT printer

provided by logic contained and the device's DMA interface module; the processor is not involved with address and data transfers during a DMA operation.

3.3.3.3 Interrupts

Any peripheral device can request an interrupt causing the processor to temporarily suspend its program execution to service the requesting device. Each device that is capable of requesting an interrupt must have a service routine which is entered when the processor acknowledges the interrupt request. Upon completion of the service routine, program control is returned to the interrupted program.

Any device that can interrupt the processor can also interrupt the service routine execution of a lower priority device if the PSW bit 7 is 0. The service routine must set this bit if it does not want to be interrupted.

An interrupt vector associated with each device is hand-wired into the device's interface/control logic. This vector is an address pointer that allows automatic entry into the appropriate service routine without device polling.

3.4 Display Description

The elimination of the standard dry-paper facsimile recorder is perhaps the most worthwhile achievement of concern herein. Although the standard recorder displays the three dimensional characteristics needed in echosonde systems, i.e., height, time and intensity, it also is messy, hard to align and maintain, and requires rather exotic writing amplifiers, writing belt drive circuits and paper drive circuits. Paper replacement is complicated, and storage and reproduction of facsimile records are very difficult.

For these and many other reasons, a modified high-speed dot-matrix impact printer is used both as the INPUT/OUTPUT (I/O) device for the microcomputer and as the facsimile recorder. An equipment search was conducted and an Applied Computer Technology (ACT) Model 950 dot-matrix impact printer was selected (Fig. 3.4.1). Although considerably more expensive than similar printers, the ACT 950 is the only one on the market that can back up the paper. By use of this capability, multiple plots can be overlaid on a single graph without complicated programming techniques.

The design of the terminal itself is based on a microcomputer controlled electrical and mechanical assembly utilizing a programmed microprocessor to control the various functions and character set of the printer. Printing is performed by a 7-wire solenoid-driven moveable printhead where the dots are placed in a 9 by 7 array to form any character or set of characters. The maximum printing speed is 120 char-

acters per second with an internal buffer memory capable of storing 320 characters. If the printer is printing asynchronously at 120 characters per second and no time is allowed for line feeds or other such functions, the incoming data will be stacked up in the buffer. When the buffer is full, a signal is generated that causes any new data to be neglected until the contents of the buffer have been printed.

The printer can be operated directly from the keyboard, or by computer control or other remote processor. In the remote mode the printer is operated through the RS-232 serial interface to the remote device and accepts ASCII coded inputs in the form of characters and non-printing tasks such as carriage returns, line feeds, etc. Thus, the capability of separating the printer from the echosonde and using acoustic couplers for remote communication exists.

Figure 3.4.2 shows the special character set produced by factory reprogramming of the printers PROM utilizing the lower case letter ASCII codes. Initially, 26 tonels were designed; the most appropriate 9 were selected by experimentation. To show the results of attempting to produce intensity records equivalent to existing facsimile recorders, actual recorded acoustic data were obtained. A suitable atmospheric event containing sharp contrasting shapes and shades was selected and processed. The quantized echo intensity levels were then displayed on the printer using different combinations of the tonels to produce the best reproduction.

Figures 3.4.3 and 3.4.4 illustrate the comparison between the facsimile record and the printer's output. Initial evidence indicates that meaningful interpretation and recognition of atmospheric processes are satisfactorily accomplished by the line printer. In addition, its versatility in the types of displays and combinations of displays with printouts indicates that future systems will include a line printer of this type. Recent literature reveals many compatible yet less expensive high-speed line printers using microprocessor control and dot-matrix impact printing.

4. ECHOSONDE SYSTEM TESTS

4.1 Graphics Design and Tests

Progress, although very slow at times because of delays in delivery of needed parts, proceeded on three fronts simultaneously, i.e., the hardware, the graphics, and finally the Doppler algorithm.

The microcomputer, printer, and miscellaneous parts were placed on order while the design and prototype layout of the ANALOG CONTROL BOARD commenced. Once completed it was installed and thoroughly tested, suffering only one minor wiring error which was easily corrected. The Digital Control Board (DCB) was designed but lack of time and parts has

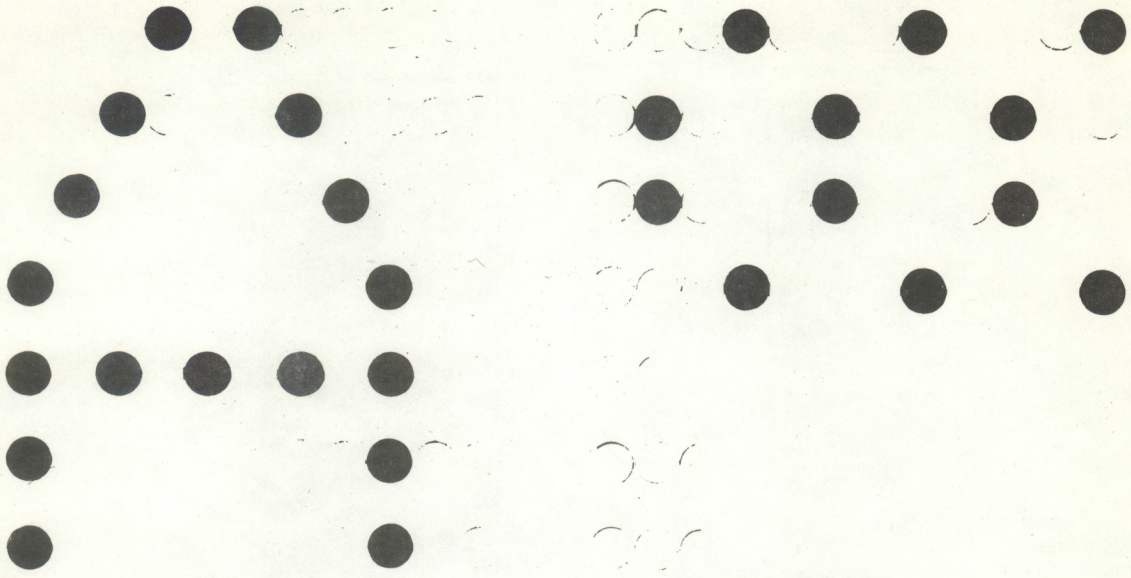

(a) Dot configuration for 'A'

(b) Dot configuration for m

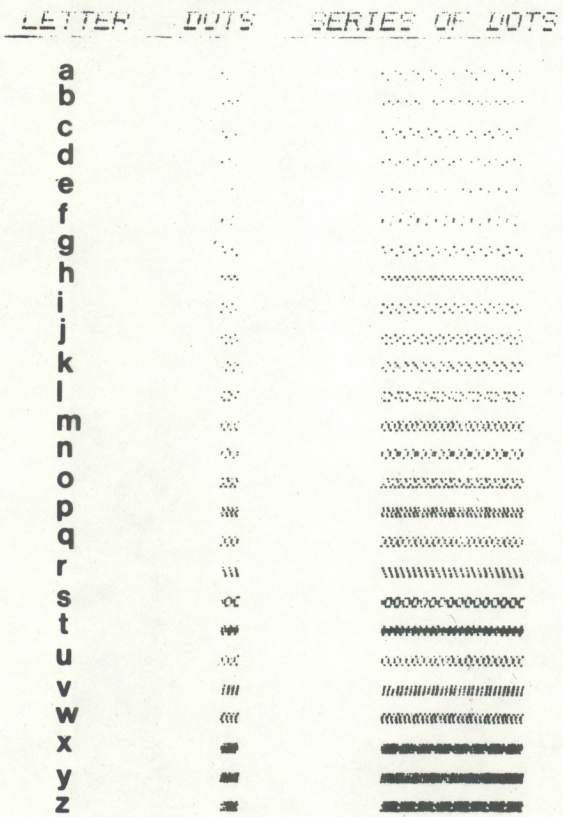

Fig. 3.4.2 Special character set.

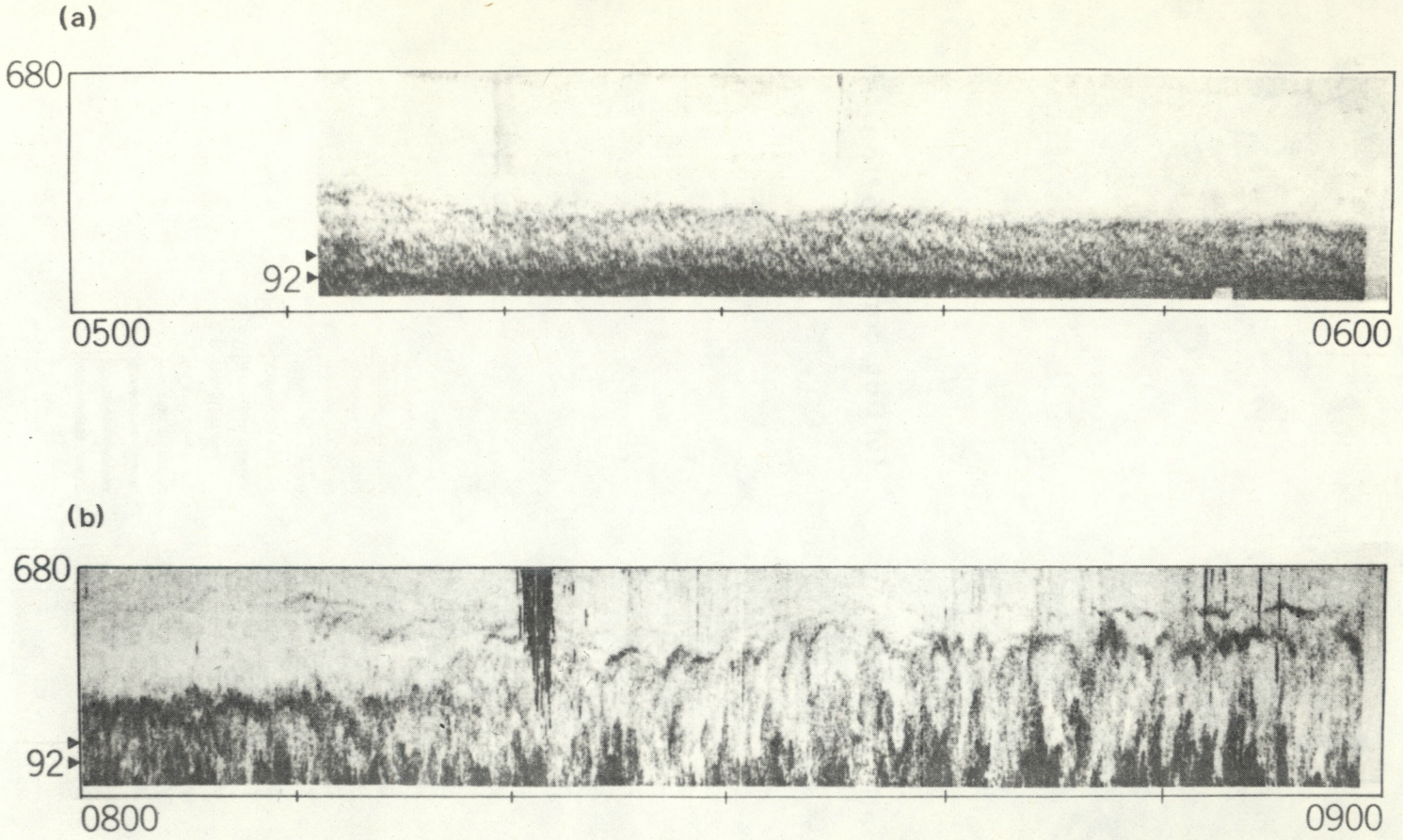

Fig. 3.4.3 Typical facsmile reeords used for comparison

(a)

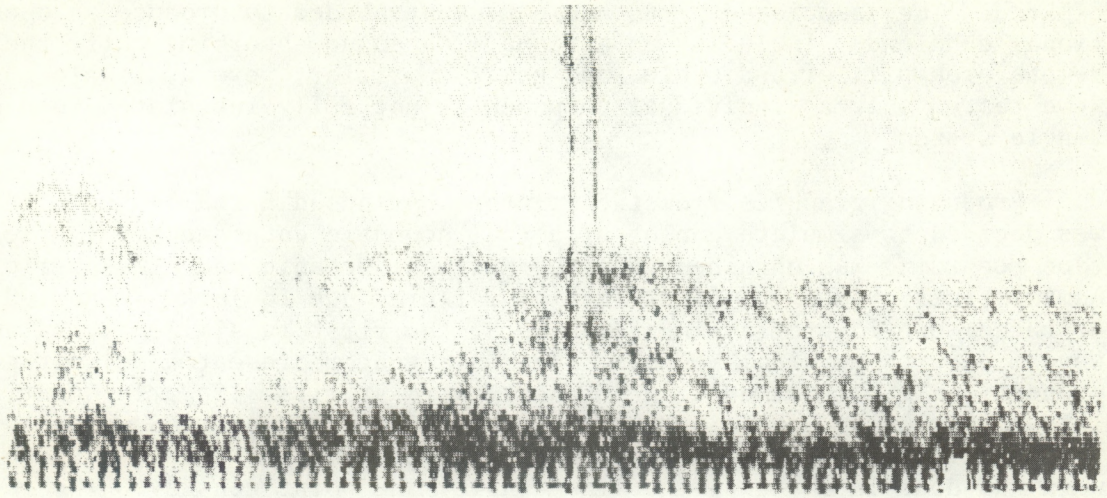

(b)

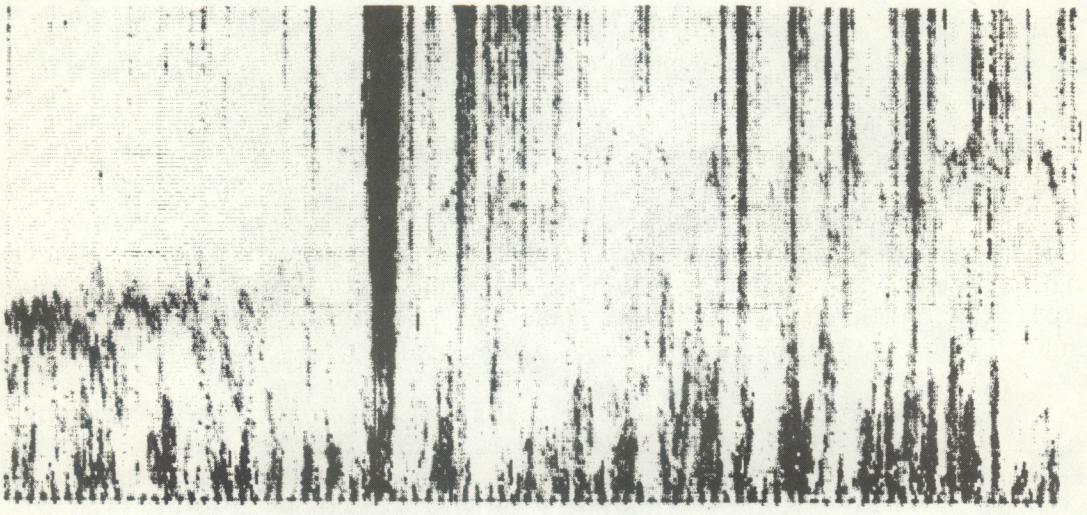

Fig. 3.4.4 PRINTER FACSIMILE RECORDS USED FOR COMPARISON

delayed its construction and testing; no appreciable problems are anticipated. The associated parts and equipment needed to produce an operational echosonde, including an antenna with sound absorbing cuff, the remote preamplifier and cable, and power amplifier, were available but were tested only as individual components, not fully integrated into a single system.

Producing graphics from the printer was indeed a challenge. It was decided to simulate a plot of actual acoustic data and a magnetic tape recording was obtained from the National Oceanic and Atmospheric Administration (NOAA). After initial failures due to lack of knowledge of rather exotic programming techniques, the first facsimile recordings were made with marginal results. The data that represent a dc voltage proportional to returned echo intensity were at first linearly quantized into the printing levels but later logarithmically quantized using 10 3.6-dB levels. The results were shown earlier in this thesis. Some work was done in changing the line density and point density. The results clearly indicate that facsimile-type records can be faithfully reproduced in this manner.

The Doppler algorithm used to calculate winds remotely is described in the next section.

4.2 Data Processing and Experimental Procedures

4.2.1 Data Description

The FFT and ADAP techniques have already been used to process echosonde data. Several comparisons with tower measurements have been reported (Keeler and Griffith, 1976). The data used for the evaluation were taken on March 24, 1974, at Haswell, Colorado. The experiment was conducted by NOAA/WPL in Boulder, Colorado.

A 150-meter instrumented meteorological tower provided reference data for an acoustic sounder (echosonde) operating 140 meters away at an azimuth of 315°. The monostatic sounder was tilted at an elevation angle of 75° away from the tower. Figure 4.2.1 shows a side view of the site configuration. Although the 75° elevation angle of the sounder is not optimal for horizontal wind sensing, it was nevertheless useable. The pulse repetition rate (PRF) was 2 seconds, creating an unambiguous range of 340 meters, and the pulse duration was 50 msec at a center frequency of 2500 Hz.

A 100-Hz bandwidth filtered version of the received echoes was heterodyned down to 250 Hz and digitized at a 1-kHz sampling rate using an effective 12-bit A/D converter. A block diagram of this system is shown in Figure 4.2.2. The time period analyzed was from 0825-0835 on March 24, 1974. A nocturnal inversion was breaking up with echoes to 240 meters and some thermal plumes to 100 meters were in the process of forming. A 4 msec wind was blowing from the SE, creating Doppler

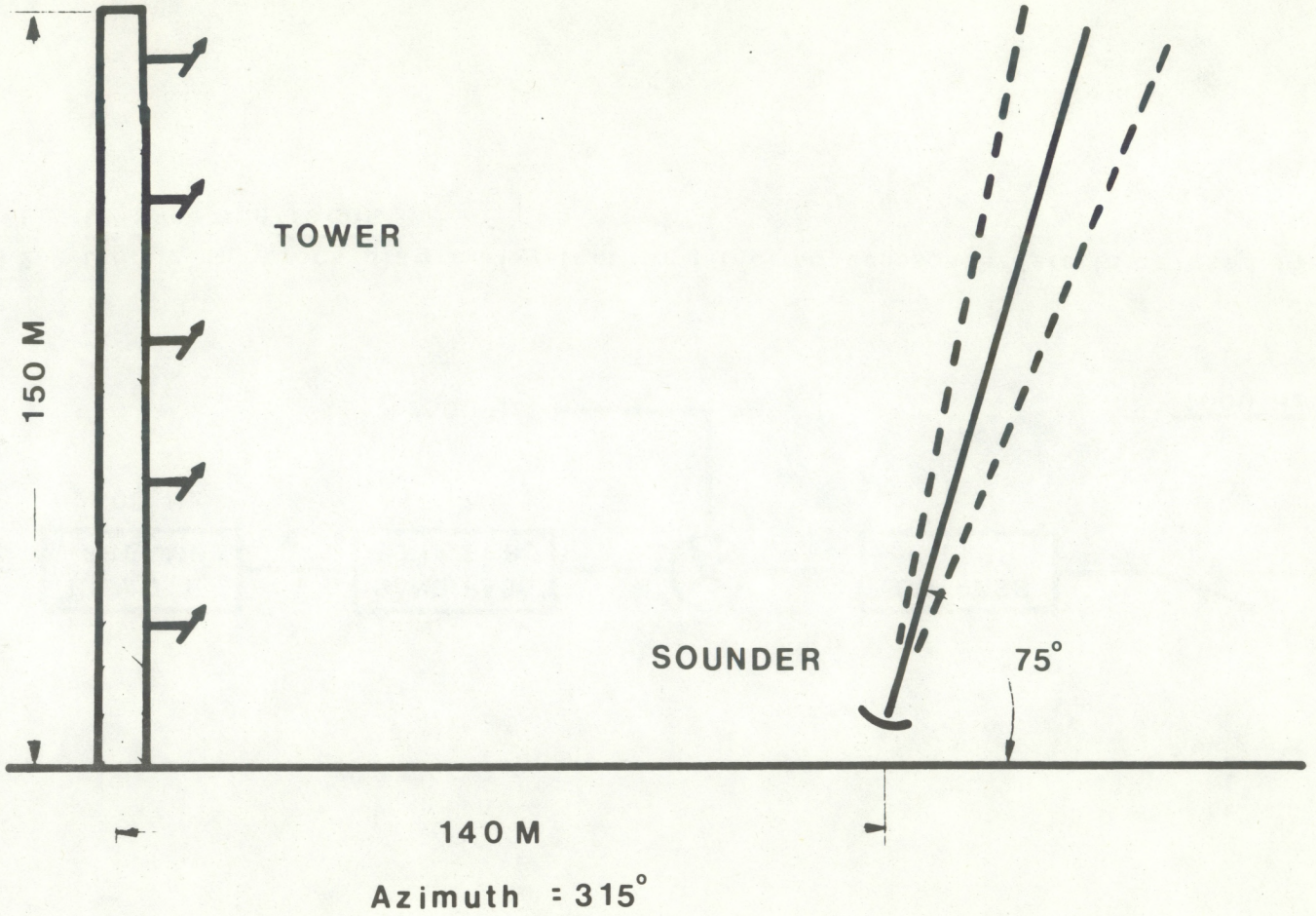

Fig. 4.2.1 Haswell 1974 acoustic sounder/tower configuration.

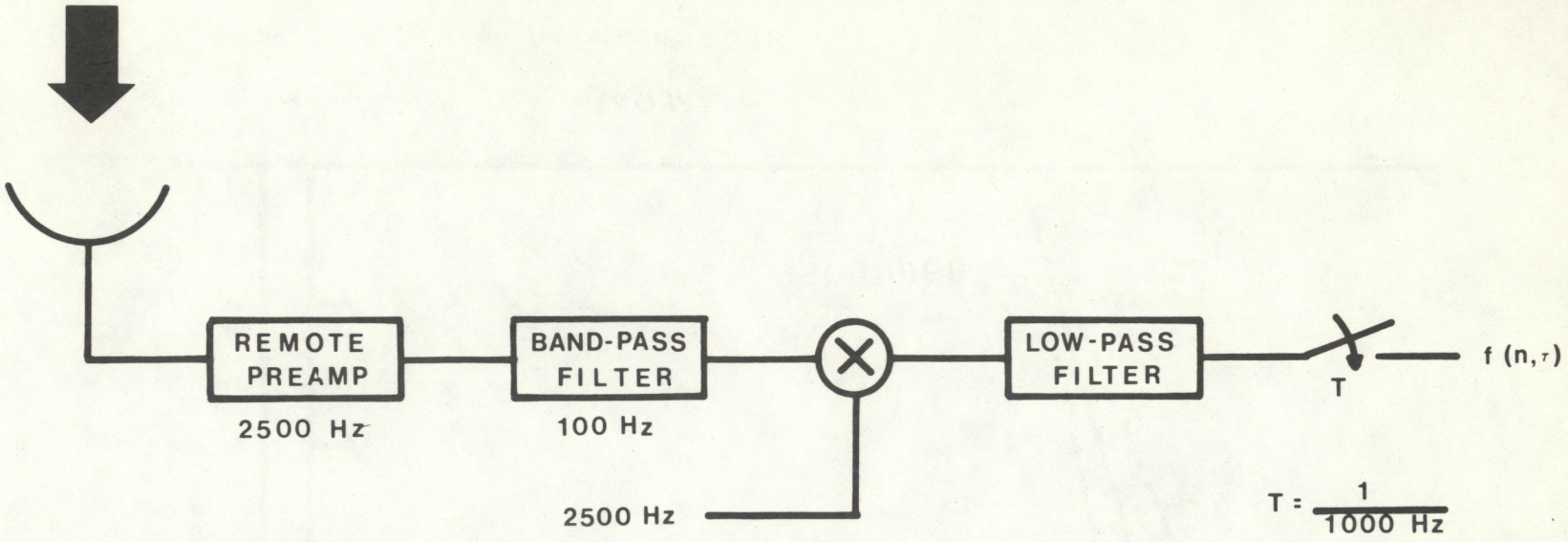

Fig. 4.2.2 Digitizing block diagram (system for gathering echosonde data to be used in this comparison).

shifts of about -15 Hz. The data analysis consisted of dividing the 2-second pulse (340 m) into 100-msec (17 m) range gates and estimating the mean Doppler shift by use of the FFT/spectrum mean, the ADAP/spectrum peak algorithm, and finally the real correlation (RC) technique.

The real correlation method does not require much computation and the entire program with an example output is shown in Figure 4.2.3. The output represents Record 10 only of the data. It was found to be quite advantageous to use this record as a benchmark to insure that all programs were operating properly.

4.2.2 Results of Computations

The calculation results shown in Tables (4.2.1), (4.2.2), and (4.2.3) represent the following: FTT IM

Prefix denotes method used	Suffix denotes averaging time
FFT - Fast Fourier transform	IM - current ray
ADAP - Adaptive filter	AV1 - exponential 10 second average
RC - Real correlation	AV2 - exponential 2 min average

Each record number represents 2 seconds of data, i.e., record 10 = 20 sec
record 150 = 5 min

The gate numbers represent 20 range gates of 100 points each.

```
PROGRAMRDP1(INPUT,OUTPUT,TAPE1)
DIMENSION IDOT(2000)
READ(1,10)IDOT
10 FORMAT(10I8)
NN=0
DO 4 I=1,20
ISUMO=0
ISUM1=0
DO 5 J=1,100
ISUMO=ISUMO+IDOT(J+NN)*IDOT(J+NN)
IF (J.GT.99)GO TO 5
ISUM1+ISUM1+IDOT(J+NN)*IDOT(J+NN+1)
5 CONTINUE
SUMO=ISUMO
SUM1=ISUM1
SUMO=(SUMO)/100.
SUM1=(SUM1)/99.
NN=NN+100
AN2=SUM1/SUMO
BN=ACOS(AN2)
PI=3.1415926
F=(500./PI)*BN)-250.
PRINT9,I,SUMO,SUM1,F
9 FORMAT(5X,*GATE=*,I3,5X,F10.3,5X,F10.3,5X,*FREQ.SHIFT=*,E10.4
4 CONTINUE
END
```

GATE NO.	R(0)	R(1)	FREQ. SHIFT (HZ)
1	411.990	28,141	-.1088E+02
2	12197.650	2283.838	-.2998E+02
3	3937.510	288.404	-.1167E+02
4	3297.400	111.677	-.5391E+01
5	1512.790	89.909	-.9465E+01
6	266.820	20.899	-.1248E+02
7	619.370	91.222	-.2353E+02
8	3267.530	182.465	-.8892E+01
9	906.280	25.384	-.4458E+01
10	3331.870	353.263	-.1691E+02
11	1924.130	205.697	-.1705E+02
12	750.630	10.737	-.2277E+01
13	2419.280	-24.636	.1621E+01
14	5261.720	214.556	-.6492E+01
15	496.370	-6.788	.2177E+01
16	235.150	-4.192	.2837E+01
17	430.240	9.717	-.3595E+01
18	656.140	11.354	-.2754E+01
19	916.680	-24.737	.4295E+01
20	1340.360	-79.535	.9450E+01

Figure 4.2.3. Real covariance computer program

Table 4.2.1. Doppler shift (Hz) for records 1-10.

Gate #	FFTIM	FFTAV1	FFTAV2	ADAPIM	ADAPAV1	ADAPAV2	RCIM	RCAV1	RCAV2
1	+5.69	+4.73	+4.15	-38.90	-19.13	-11.52	-10.88	-1.92	+0.57
2	-28.61	-17.22	-13.49	-42.05	-29.30	-24.86	-29.98	-19.82	-16.81
3	-14.83	-4.55	-2.49	-26.18	-7.09	-2.44	-11.67	-3.52	-1.03
4	-6.02	-2.46	-2.33	-23.14	-5.03	-4.23	-5.39	-3.84	-3.02
5	-10.69	-6.87	-6.58	-13.84	-7.65	-7.31	-9.46	-7.06	-7.54
6	-12.22	-5.31	-5.00	-20.82	-8.45	-7.96	-12.48	-6.04	-6.26
7	-27.67	-13.92	-11.16	-19.81	-13.92	-12.29	-23.53	-11.86	-10.26
8	-4.61	-10.18	-10.84	-0.58	-10.46	-12.46	-8.89	-10.51	-11.07
9	-9.75	-7.04	-5.92	-14.43	-8.17	-6.53	-4.46	-9.12	-9.09
10	-12.00	-9.06	-8.38	-13.97	-8.99	-8.11	-16.91	-9.42	-8.34
11	-10.58	-9.65	-8.69	-17.40	-11.29	-9.86	-17.05	-11.66	-10.39
12	-6.48	-5.71	-5.35	+4.74	-0.92	-1.04	-2.28	-5.64	-4.91
13	-4.58	-5.22	-5.53	+1.28	-3.02	-3.52	+1.62	-2.70	-3.59
14	-6.74	-1.21	-1.73	-4.39	+2.55	+1.67	-6.49	-1.09	-0.30
15	+2.25	-4.27	-4.82	+1.53	-8.58	-8.98	+2.18	-7.07	-8.41
16	+14.39	+13.78	+13.90	+5.35	-8.69	-6.32	+2.84	-7.13	-6.02
17	-8.24	-8.27	-9.32	-12.04	-12.11	-11.06	-3.59	-7.22	-7.07
18	-0.19	-5.79	-7.17	+11.17	-2.03	-5.31	-2.75	-6.26	-6.96
19	-3.87	+3.55	+4.18	+6.81	-7.23	-8.74	+4.30	-4.33	-5.55
20	+2.45	-6.36	-7.37	+11.32	-5.88	-6.53	+9.45	-5.91	-7.02

Table 4.2.2. Doppler shift (Hz) for records 1-150.

Gate #	FFTIM	FFTAV1	FFTAV2	ADAPIM	ADAPAV1	ADAPAV2	RCIM	RCAV1	RCAV2
1	-1.17	+2.73	+2.51	-17.11	-18.69	-21.58	-6.82	-6.82	-0.45
2	-10.61	-18.33	-23.41	-17.46	-19.27	-23.49	-17.49	-14.89	-13.31
3	-29.46	-17.66	-10.76	-37.29	-22.13	-10.03	-31.83	-17.77	-7.39
4	-14.41	-17.17	-10.80	-18.20	-18.65	-11.28	-14.56	-18.10	-10.37
5	-11.54	-15.73	-11.52	-23.72	-19.80	-12.84	-17.21	-16.46	-12.21
6	-14.02	-14.71	-11.55	-13.92	-19.80	-13.97	-20.08	-17.12	-12.00
7	-23.26	-18.55	-13.37	-26.18	-19.39	-14.57	-24.07	-16.45	-12.95
8	-17.86	-16.96	-12.57	-33.49	-25.80	-14.61	-19.25	-15.74	-11.99
9	-18.70	-16.13	-12.71	-19.52	-19.67	-13.58	-12.01	-17.08	-11.89
10	-18.55	-15.80	-11.28	-17.17	-16.80	-14.37	-14.63	-14.98	-11.68
11	-13.14	-13.21	-12.01	-13.07	-16.99	-13.70	-7.24	-11.87	-12.32
12	-17.36	-12.67	-10.40	-25.59	-14.72	-10.82	-13.89	-9.76	-10.14
13	-12.61	-12.83	-9.70	+5.22	-13.41	-11.06	-12.38	-10.22	-8.69
14	-10.74	-8.49	-6.41	-29.81	-12.39	-7.08	-20.02	-11.77	-6.96
15	-6.04	-4.97	-4.50	-29.82	-17.83	-7.13	-1.80	-12.37	-6.08
16	-2.78	-5.92	-0.78	+12.80	-9.08	-7.32	-2.91	-5.23	-4.39
17	-33.27	-25.57	-15.18	-17.55	-24.94	-9.93	-27.73	-19.44	-7.08
18	-20.17	-18.29	-10.79	-18.25	-8.97	-6.98	-12.82	-2.89	-4.30
19	-27.09	-22.51	-13.12	-43.97	-26.01	-9.49	-27.04	-13.24	-5.51
20	-11.86	-18.47	-9.86	+31.24	-3.54	-7.47	-7.94	-6.95	-6.06

The tower data are shown in Table 4.2.3.

Table 4.2.3. Haswell tower data, March 24, 1974 (0825 to 0835), Tape # CO419 (NOAA).

Time (m sec)	Freq Shift (Hz)
182	-11.27
366	-12.99
548	-11.89
730	-14.97
920	-15.95

4.2.3 Comparison of Results

The results of the various comparisons are shown in Figures 4.2.4 through 4.2.7.

Figures 4.2.4a - 4.4.4c (records 1-10) show the various methods on a comparative basis within each technique. The variation and effects of averaging pulse-to-pulse is clearly shown over the first 10 records.

Figures 4.2.5a - 4.2.5c (records 1-10) show that there is close agreement between all of the methods except for one "spike" point of the FFT.

Figures 4.2.6a - 4.2.6c (records 1-150) show a comparison within each technique between immediate estimation and averaging.

Figures 4.2.7a - 4.2.7c (records 1-150) show that even though there is quite a pulse-to-pulse variation in spectra the averages of each of the methods appear to converge quite nicely. Figure 4.2.7c represents a comparison using a 2-minute exponential average over 5 minutes.

4.2.4 Conclusions and General Discussion of Data Processing Results

The implementation of the correlation methods can be accomplished with a great savings in both time and hardware. For example, using as a basis the Digital Equipment LSI-11 microprocessor the following is an estimate of the time required to compute one range gate of data composed of N = 100 points.

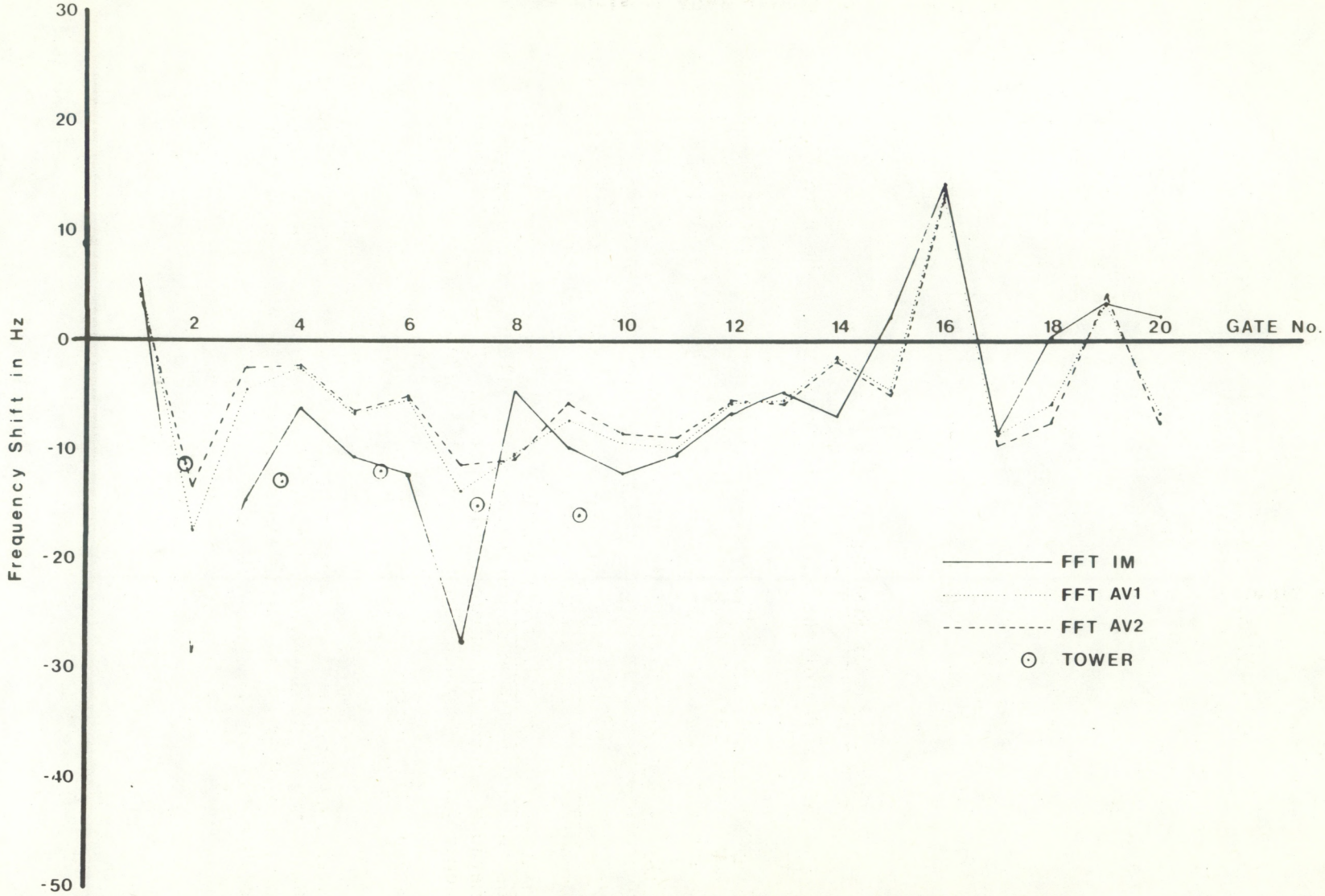

Figure 4.2.4a Plots of FFT results of Record No.10

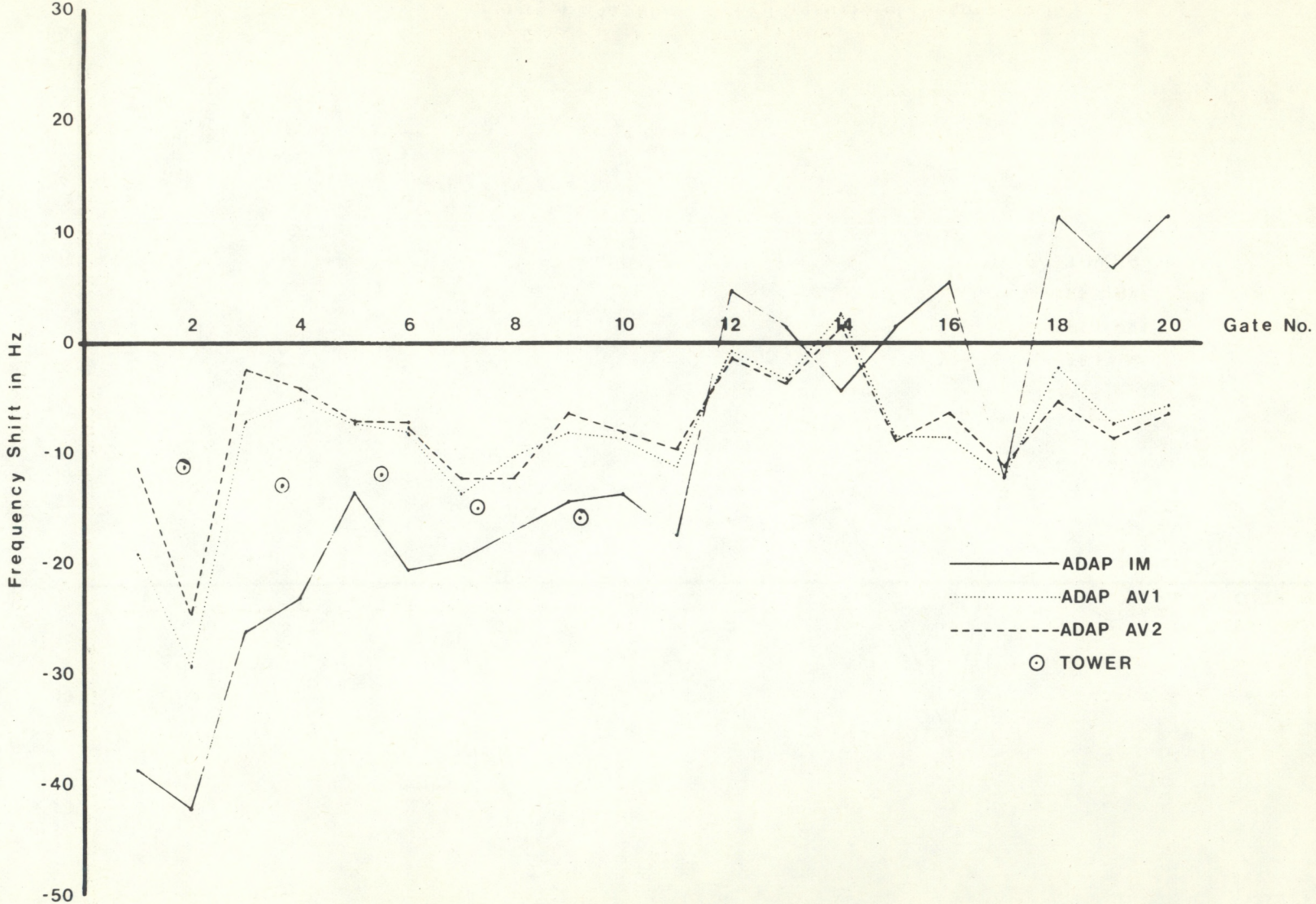

Figure 4.2.4b Plots of ADAP results of Record No.10

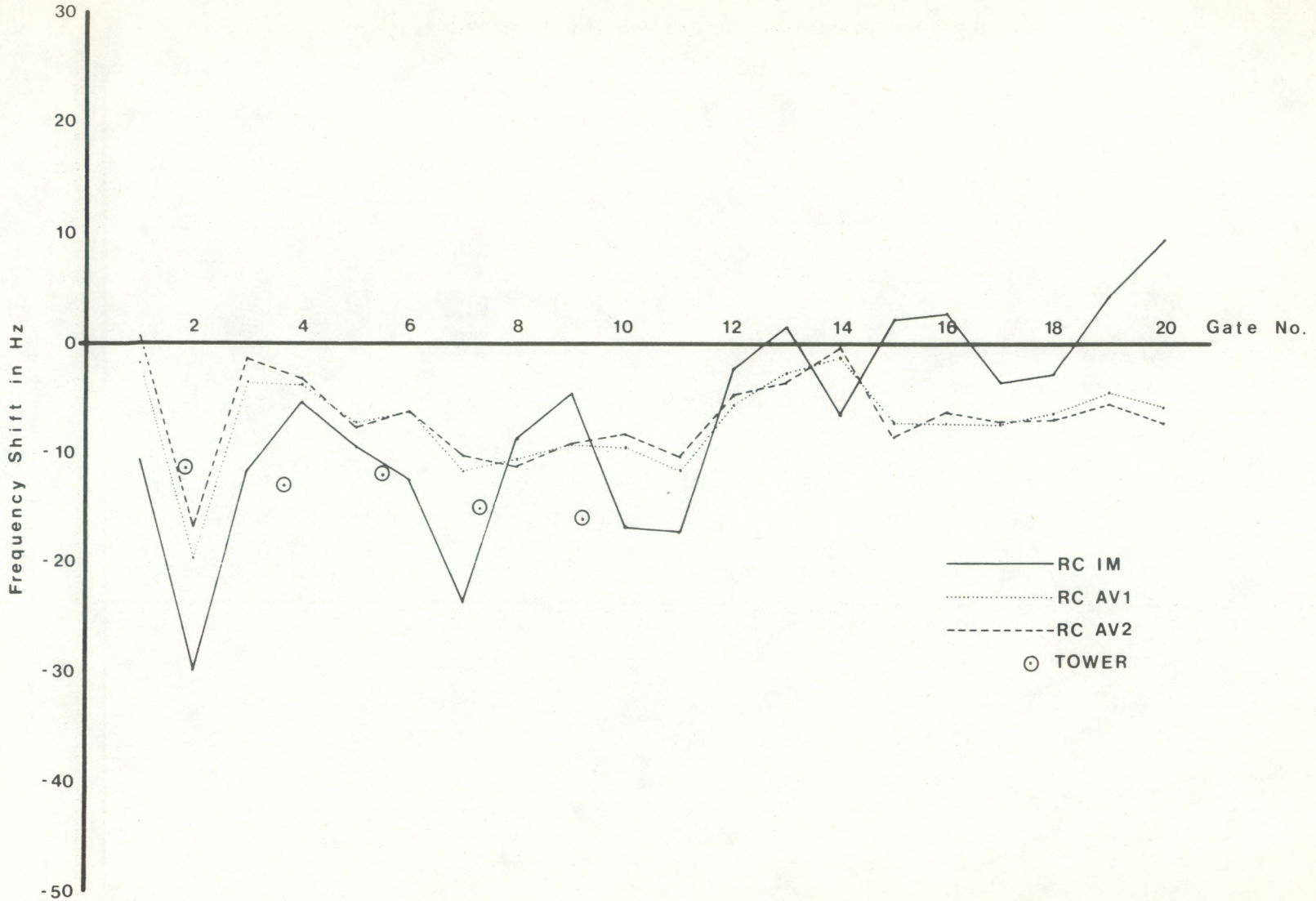

Figure 4.2.4 c Plots of RC results of Record No.10

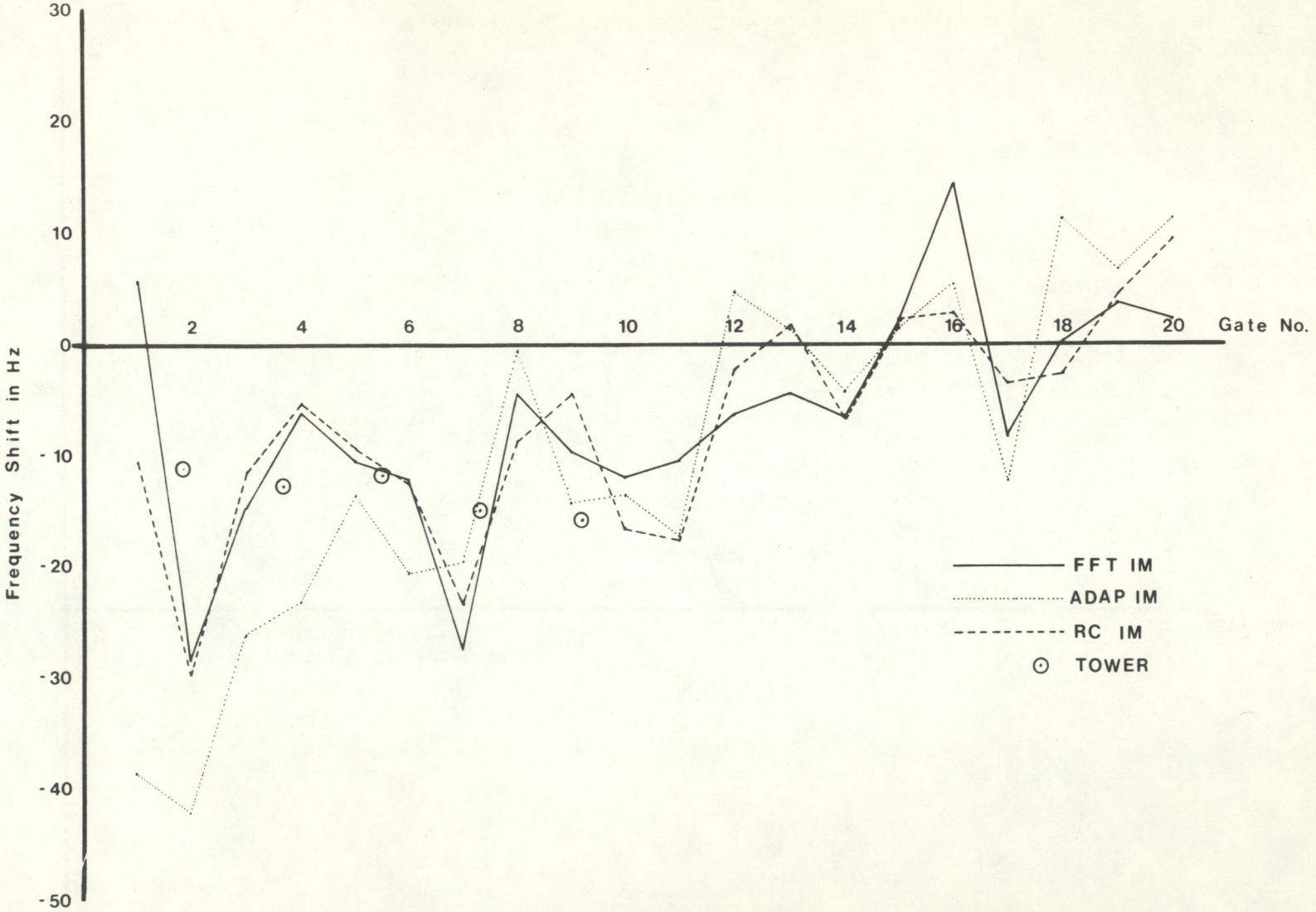

Figure 4.2.5 a Plots of IM results of Record No. 10

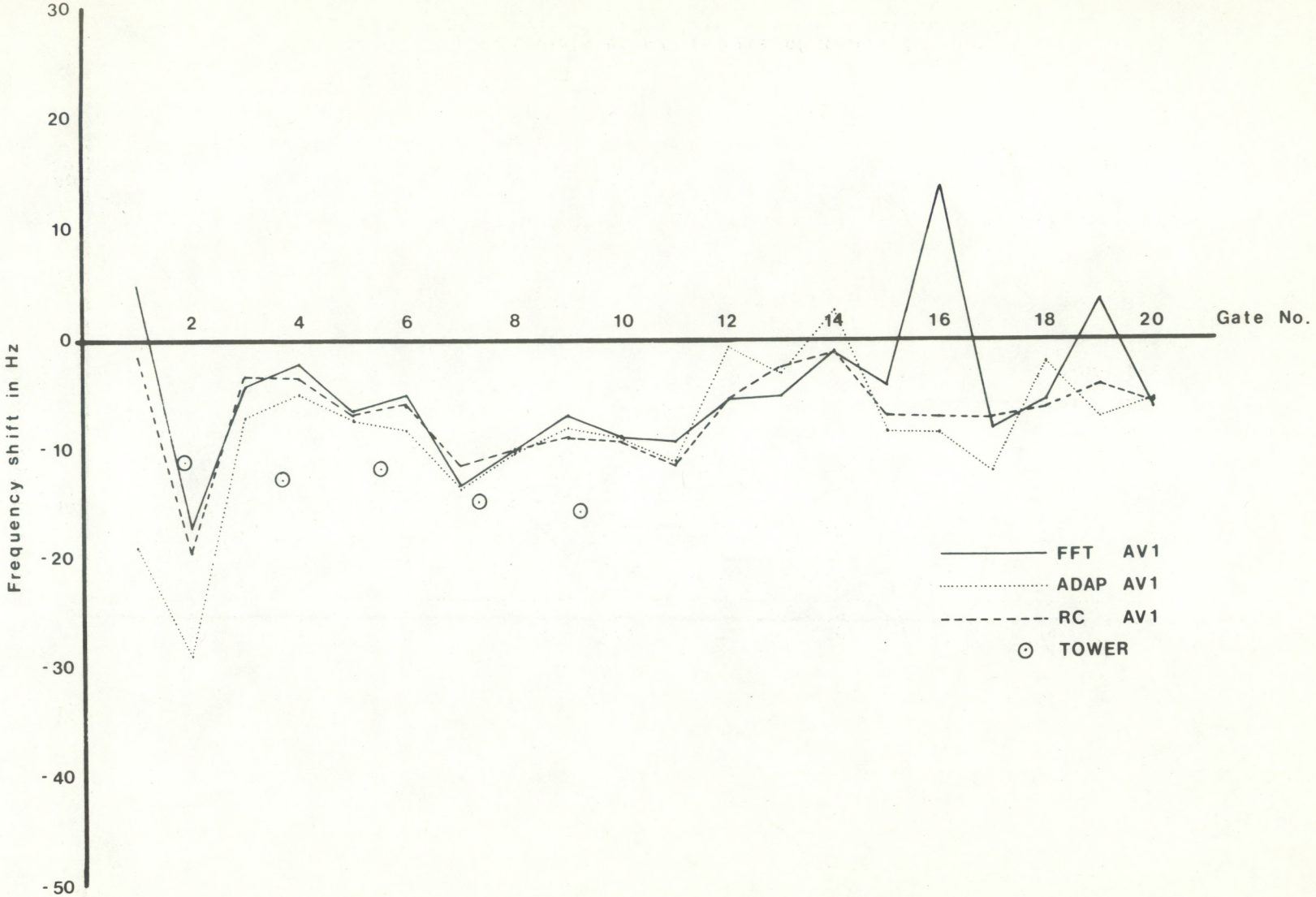

Fig. 4.2.5b Plots of AV1 results of Record No. 10

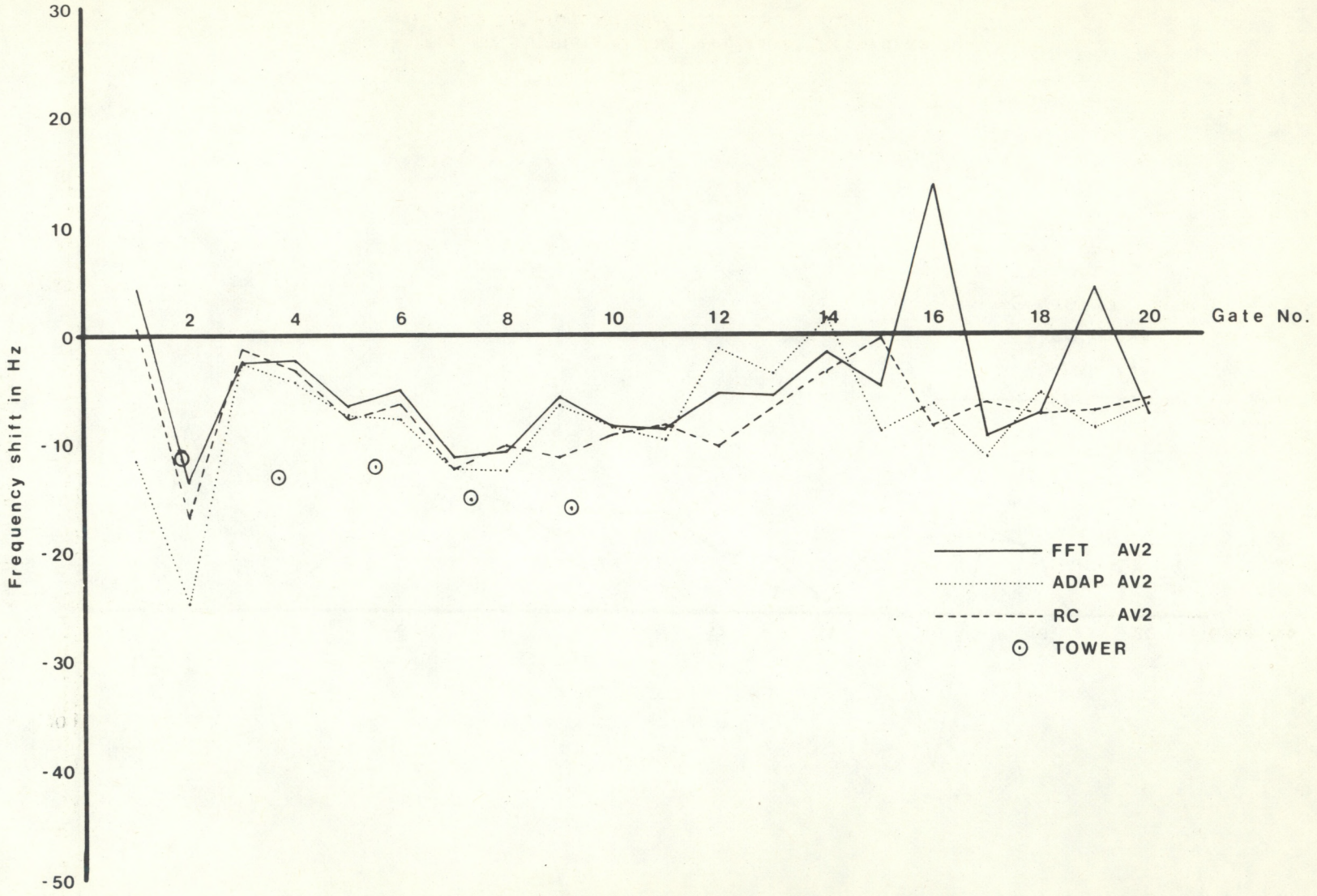

Fig. 4.2.5 Plots of AV2 results of Record No. 10

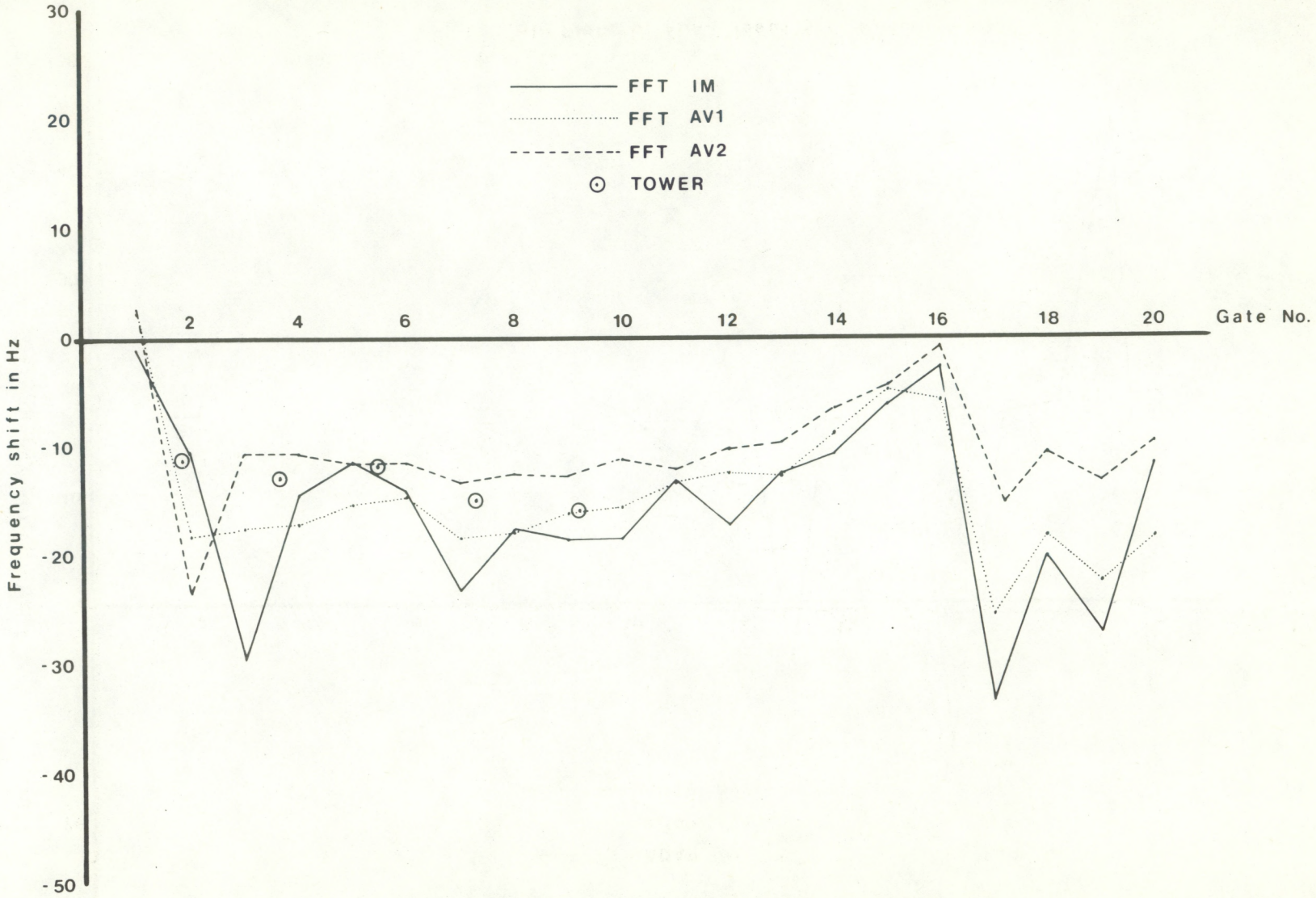

Fig. 4.2.6a Plots of FFT results of Record No. 150

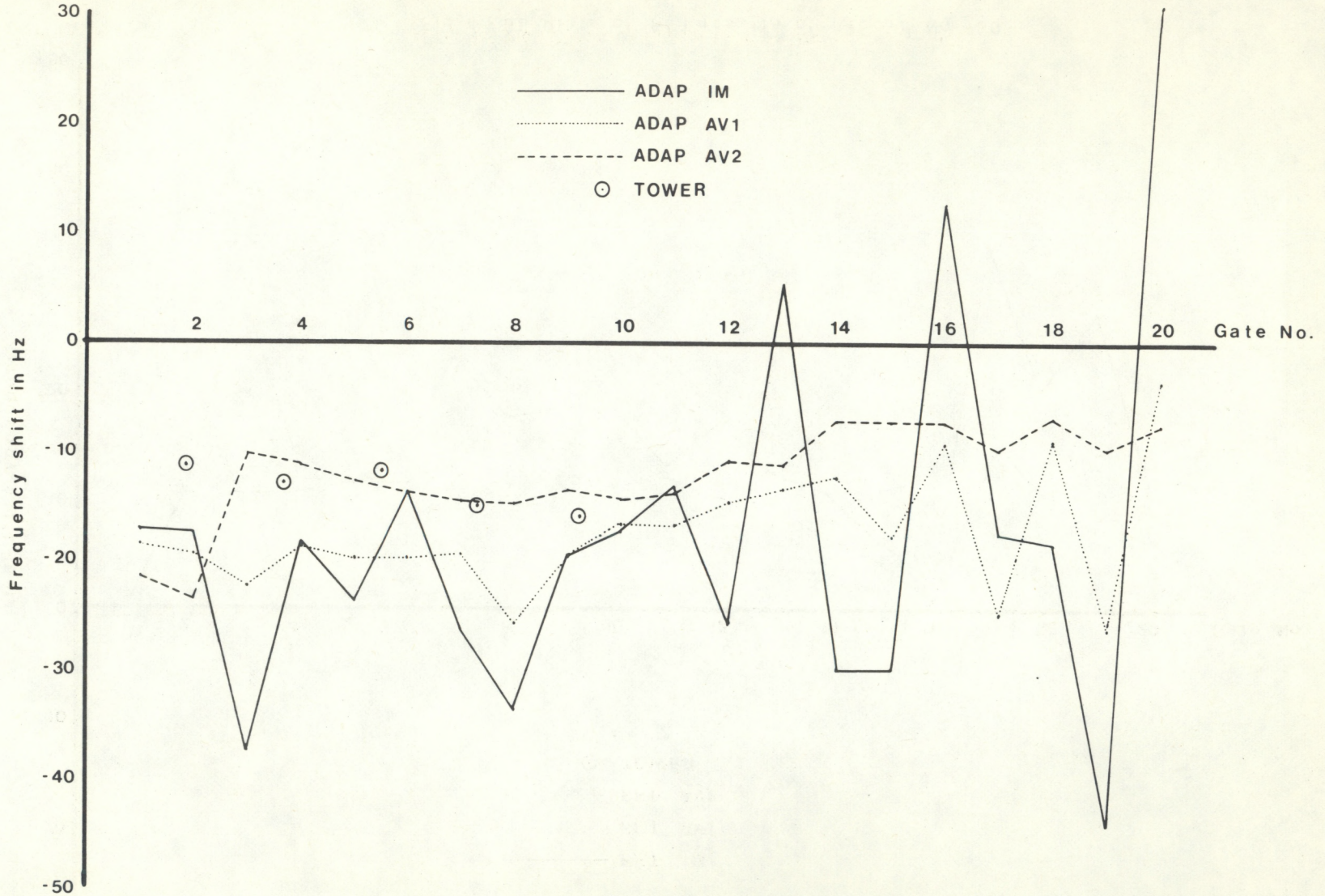

Fig. 4.2.6b Plots of ADAP results of Record No. 150

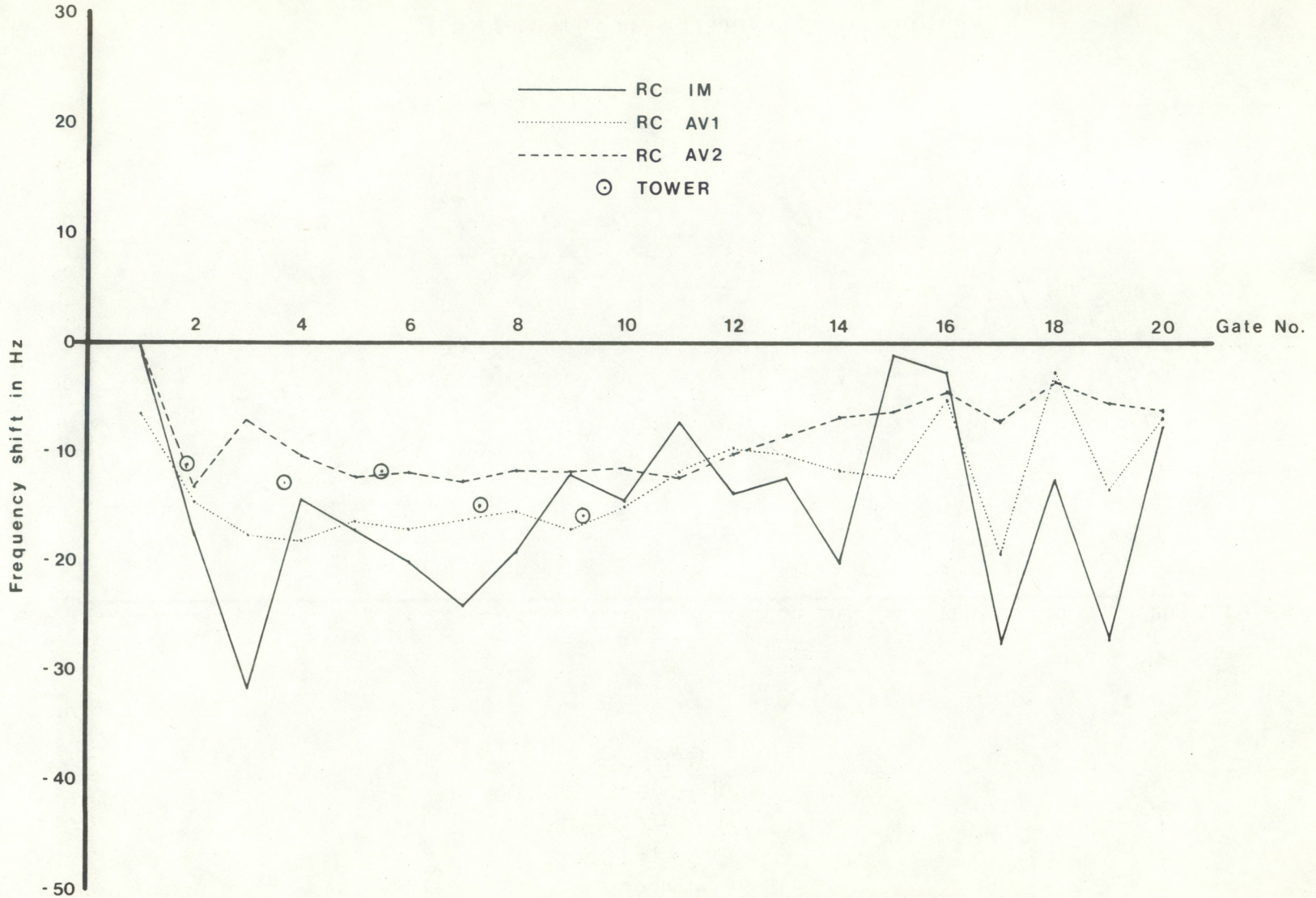

Fig. 4.2.6c Plots of RC results of Record No. 150

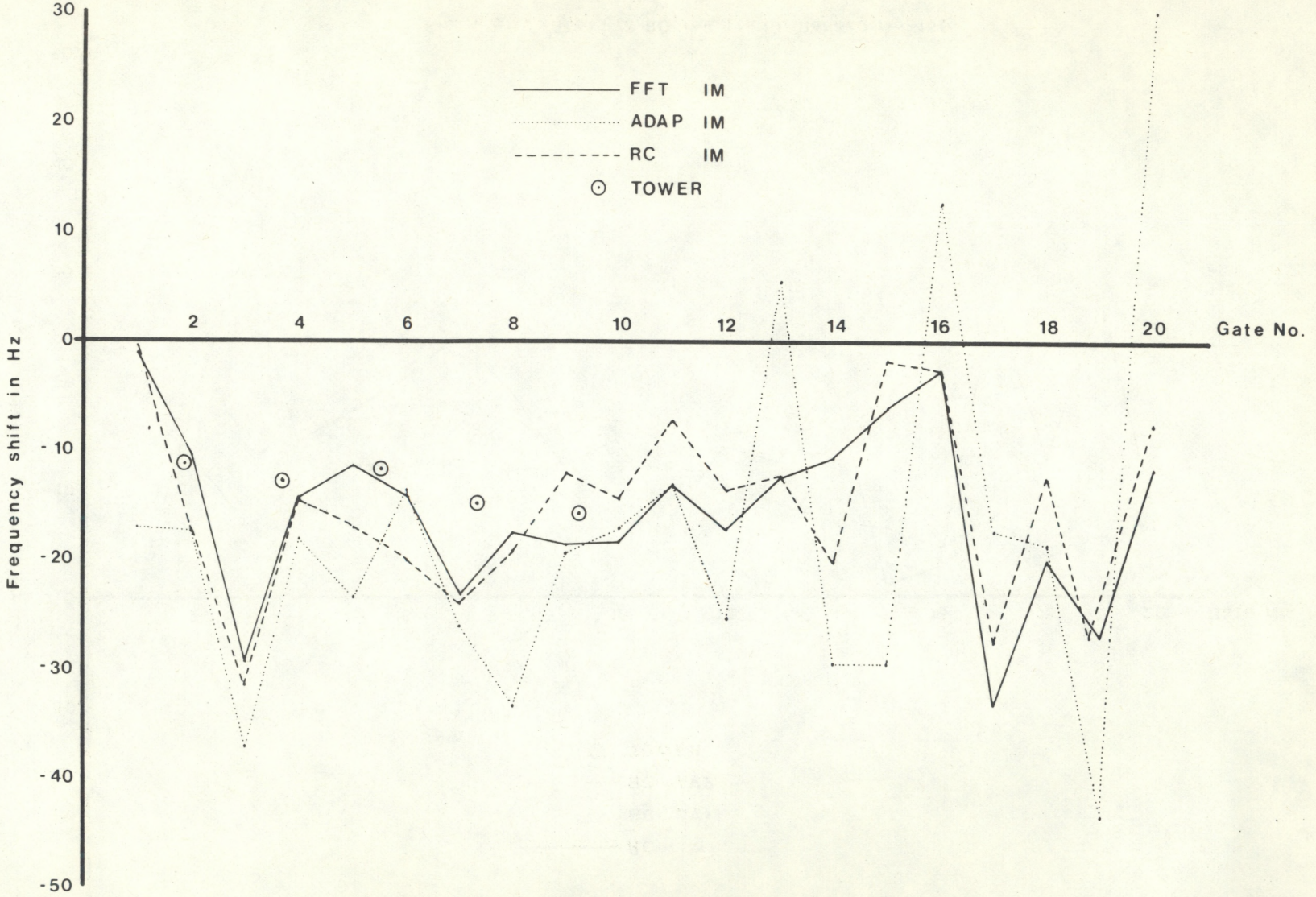

Fig. 4.2.7a Plots of IM results of Record No. 150

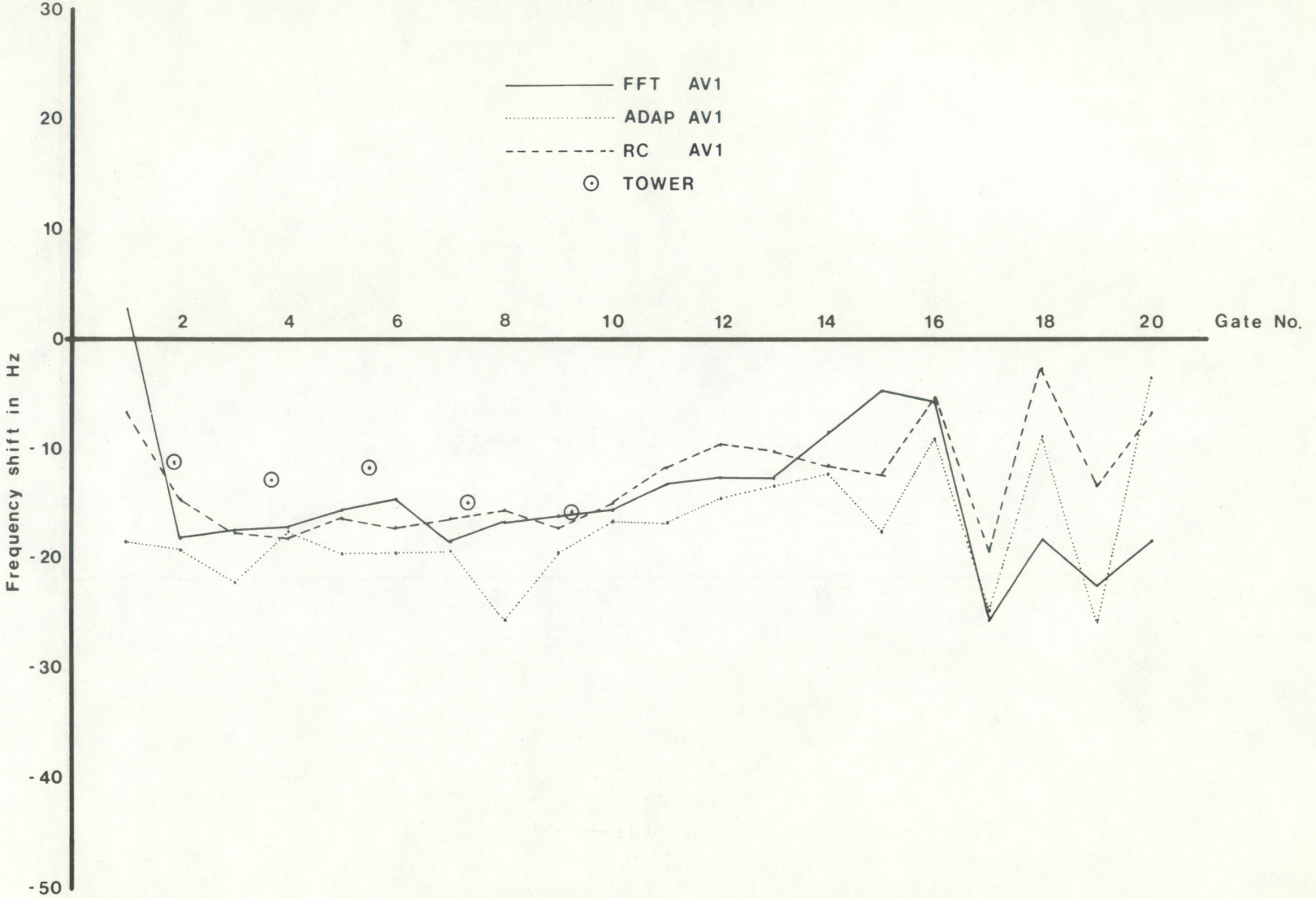

Fig. 4.2.7b Plots of AV1 results of Record No. 150

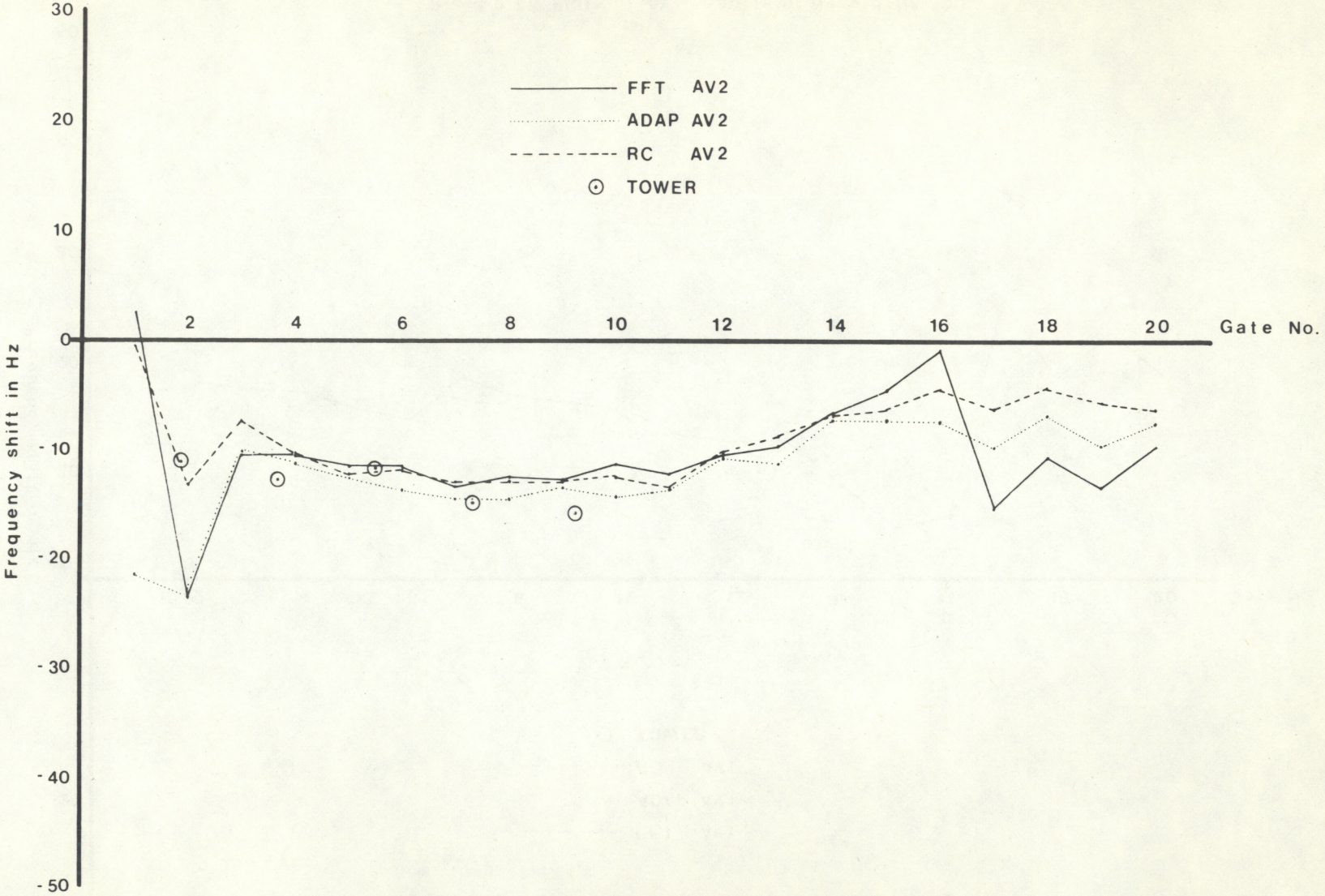

Fig. 4.2.7c Plots of AV2 results of Record No.150

$$\hat{R}(0) = \frac{1}{N} \sum_{n=1}^{N} X(n)X(n)$$

adds (+) = 100 @ 4μsec = 400μsec

multiply (x) = 100 @ 31μsec = 3100μsec

divides (÷) = 1 @ 78μsec = 78μsec

Subtotal 3578μsec

$$\hat{R}(1) = \frac{1}{N-1} \sum_{n=1}^{N-1} x(n)x(n+1)$$

adds (+) = 99 @ 4μsec = 396μsec

multiply (x) = 99 @ 31μsec = 3069μsec

divides (÷) = 1 @ 78μsec = 78μsec

Subtotal 3543μsec

The computation of the mean frequency also requires an arc-cos function that can be easily computed from either a table look-up or a series expansion. Assume that a series is used where

$$\cos^{-1}x = \pi/2 - (x + \frac{x^3}{6} + \ldots +).$$

This value must be computed once per gate to obtain the mean frequency estimate. Assume terms up to $\frac{x^3}{6}$; then

adds (+) = 2 @ 4μsec = 8μsec

multiply (x) = 2 @ 31μsec = 62μsec

divides (÷) = 1 @ 78μsec = 78μsec

Subtotal 148μsec

Consider as an example the real correlation output shown in Figure 4.2.3 range gate #5, where

$$\frac{\hat{R}(1)}{\hat{R}(0)} = \frac{89.91}{1512.79}$$

$$\hat{f} = \frac{500}{\pi} \cos^{-1}(.05943) - 250$$

$$\hat{f} \approx \frac{500}{\pi} \left[\frac{\pi}{2} - (.05943) + \left(\frac{.05943}{6}\right)^3\right] - 250$$

$$= -9.46$$

The time required on the LSI-11 should be less than 3.6 + 3.5 + 0.1 = 7.2 msec and for 20 such gates the time should be less than 144 msec. This indicates that it should be possible to calculate and display a total 3-axis Doppler system (even with a pulse repetition rate of less than 1 second) in real time.

The hardware realization of this method is quite straightforward requiring only a sampler and an A/D converter operating with a microprocessor such as the DEC LSI-11.

It should also be noted that storage requirements for the correlation method are fewer than for the other methods. The programs are quite simple and very little intermediate storage is needed during the calculations. This is in contrast to ADAP if one desires to compute the mean frequency in a "reverse" data sequence (Keeler and Griffith, 1976).

5. DISCUSSION AND RECOMMENDATIONS

The analysis and design of an echosonde utilizing advanced analog and digital circuits, a microcomputer based operating and control system, and a real covariance digital signal processing scheme were performed in detail. Historical theoretical analysis was used to develop the equations for temperature (C_T) and velocity (C_V) profiles thus making use of the Doppler shift of the returned echo signal as well as its intensity. A new and novel technique was developed for calculating the spectra of the Doppler shift (thus the associated wind speed) in real time on a microcomputer. The real covariance algorithm was implemented and tested using a computer simulation on actual echosonde data with excellent results. Finally, facsimile recordings of actual echosonde recordings of echo intensity were reproduced on a special character high-speed printer and compared against the original with very satisfactory results.

RECOMMENDATIONS

A number of potential uses of this echosonde would be highly advantageous. For instance, the device could be used for air pollution monitoring and control growing concerns especially in the larger cities. At the same time, it could be used to justify relaxing air pollution controls during certain advantageous meteorological conditions. Many users would be interested in a basic system displaying the mixing layer depth and vertical wind velocity as a function of height. Other users, could expand the system with the addition of two antennas and then calculate and display the horizontal wind field above an airport for instance.

Perhaps the most important area where further study could prove fruitful is the development of computer pattern recognition algorithms capable of determining and even predicting temperature inversion height and relative intensity. Computer aided decision-making programs could then be developed to control the smoke-stack output and other related objectives.

Another area in which additional study would be beneficial is the general subject of enhanced signal-to-noise ratios by noise subtraction and signal validity testing using associated digital methods. Testing and possibly recording generated data to prove and improve reliability are essential.

Also, further experimentation with the tonels generated by the line printer is indicated. The technique using blocks of dots has proved effective. An alternative method uses individual dots placed at selected points on the record by a "smart" processor.

The challenge for creative use of these processes is a reality with this technology.

REFERENCES

Beran, D. W., 1971, Acoustics: A new approach for monitoring the environment near airports. J. Aircraft 11, pp. 934-936.

Beran, D. W., and S. F. Clifford, 1972, Acoustic Doppler measurements of the total wind vector. IInd Symposium on Meteor. Obs. and First Am. Meteor. Soc., San Diego, Calif., March 27-30, pp. 100-109.

Berân, D. W., and B. C. Willmarth, 1971, Doppler winds from a bistatic acoustic sounder. Proc. Seventh Int. Symp. on Remote Sensing of the Environment, Univ. of Michigan, 3, pp. 1699-1714.

Beran, D. W., F. F. Hall, J. W. Wescott, and W. D. Neff, 1971, Applications of an acoustic sounder to air pollution monitoring. Presented at the Air Pollution Turbulence and Diffusion Symposium December 7 - 10, 1971 at the New Mexico State University, Las Cruces, New Mexico, p. 7.

Beran, D. W., W. H. Hooke, and S. F. Clifford, 1973, Acoustic echo-sounding techniques and their application to gravity-wave, turbulence, and stability studies. Boundary-Layer Meteorol. 4, pp. 133-153.

Beran, D. W., C. G. Little, and B. C. Willmarth, 1971, Acoustic Doppler measurements of vertical velocities in the atmosphere. Nature 230, pp. 160-162.

Beran, D. W., B. C. Willmarth, F. C. Carsey, and F. F. Hall, Jr., 1974, An acoustic Doppler wind measuring system. J. Acoust. Soc. Am., 55, No. 2, pp. 334-338.

Blackman, R. B., and J. W. Tukey, 1958, The measurement of power spectra. Dover Publications, New York.

Brown, E. H., 1972, Acoustic-Doppler-radar scattering equation and general solution. J. Acoust. Soc. Am., 52, No. 5 (Part 2), pp. 1391-1396.

Brown, E. H., and R. J. Keeler, 1975, Applications of propagation parameters to atmospheric echosondes. Proc. 16th Radar Meteorol. Conf., Amer. Meteorol. Soc.

Chadwick, R. B., and C. G. Little, 1973, The comparison of sensitivities of atmospheric echo sounders. Remote Sensing of Environ. 2, pp. 223-239.

Georges, T. M., and S. F. Clifford, 1972, Acoustic sounding in a refracting atmosphere. J. Acoust. Soc. Am., 52, No. 5 (Part 2), pp. 1397-1405.

Gilman, G. W., H. B. Coxhead and F. H. Willis, 1946, Reflection of sound signals in the troposphere. J. Acoust. Soc. Amer., 18, pp. 274-283.

Hall, F. F., Jr., 1971, Acoustic remote sensing of temperature and velocity structure in the atmosphere, Statistical Methods and Instrumentation in Geophysics, A. G. Kjelaas, ed. Teknologisk Forlag A/S, pp. 167-180.

Hall, F. F., Jr., 1972, Temperature and wind structure studies by acoustic echo sounding, Chap. 18, Remote Sensing of the Troposphere, NOAA/ERL, U.S. Govt. Printing Office, Washington, D.C.

Hall, F. F., and J. W. Wescott, 1974, Acoustic antennas for atmospheric echo sounding. J. Acoust. Soc. Am. 56, pp. 1376-1382.

Keeler, R. J., and L. J. Griffith, 1976, Acoustic Doppler extraction by adaptive inverse filtering. To be published.

Kleppe, J. A., 1975, A complex correlation approach to spectral moment estimation for Doppler echosonde data. Private Proposal by Scientific Engineering Systems, Reno, Nevada.

Kleppe, J. A., 1976, Real and complex correlation methods as applied to spectral moment estimation for Doppler echosonde data. Report to NOAA, ERL, August, 1976.

Mandics, P. A., and E. J. Owens, 1975, Observations of the marine atmosphere using a ship-mounted acoustic echo sounder. J. Appl. Meteor. 14, No. 6, pp. 1110-1117.

Mandics, P. A., E. J. Owens, and F. F. Hall, Jr., 1975, Observations of the tropical marine atmosphere using an acoustic echo sounder during GATE, Preprint Volume, 16th Radar Meteor. Conf., April 22-24, 1975, Houston, Texas. Published by Amer. Meteor. Soc., Boston, Mass.

McAllister, L. G., J. R. Pollard, A. R. Mahoney, and P. J. R. Shaw, 1969, Acoustic Sounding - A new approach to the study of atmospheric structure. Proc. IEEE, 57, 579-587.

Neff, W. D., 1975, Quantitative evaluation of acoustic echoes from the planetary boundary layer, NOAA Tech. Report ERL 322-WPL 38.

Novick, L. R., and K. M. Glover, 1975, Spectral mean and variance estimation via pulse pair processing. Preprints 16th Radar Meteorology Conference, Houston, Amer. Meteor. Soc. 1-5.

Ottersten, H., K. R. Hardy, and C. G. Little, 1973. Radar and sonar probing of waves and turbulence in statically stable clear-air-layers. Boundary Layer Meteor. 4, pp. 47-89.

Owens, E. J., 1974, Development of a portable acoustic echosounder. NOAA Tech. Report ERL 298-WPL-31, 41 pp.

Owens, E. J., 1975, NOAA Mark VII Acoustic Echo Sounder. NOAA Tech. Mem. ERL WPL-12, 71 pp.

Parry, H. D., and M. J. Sanders, 1972, The design and operation of an acoustic radar. IEEE Trans. Geosci. Electr., GE-10, No. 1, pp. 53-64.

Simmons, W. R., J. W. Wescott, and F. F. Hall, Jr., 1971, Acoustic echo sounding as related to air pollution in urban environments, NOAA Tech. Report ERL 216-WPL 17, 77 pp.

Sirmans, D., and B. Bumgarner, 1975, Estimation of spectral density mean and variance by covariance argument techniques. Proc. 16th Radar Meteorol. Conf., Amer. Meteorol. Soc.

Sirmans, D., and R. J. Doviak, 1973, Meteorological radar signal intensity estimation, NOAA TM ERL-NSSL-64.

Tombach, I., P. B. MacCready, and L. Baboolal, 1973. Use of a monostatic sounder in air pollution diffusion estimates. IInd Int. ISA Conf. Sens. Env. Pollutants, December 10-12, Washington, D.C.

Wyckoff, R. J., D. W. Beran, and F. F. Hall, Jr., 1973, A comparison of the low-level radiosonde and the acoustic echo sounder for monitoring atmospheric stability. J. Appl. Meteorol. 12.

APPENDIX A ANALOG CONTROL BOARD SCHEMATIC DIAGRAM

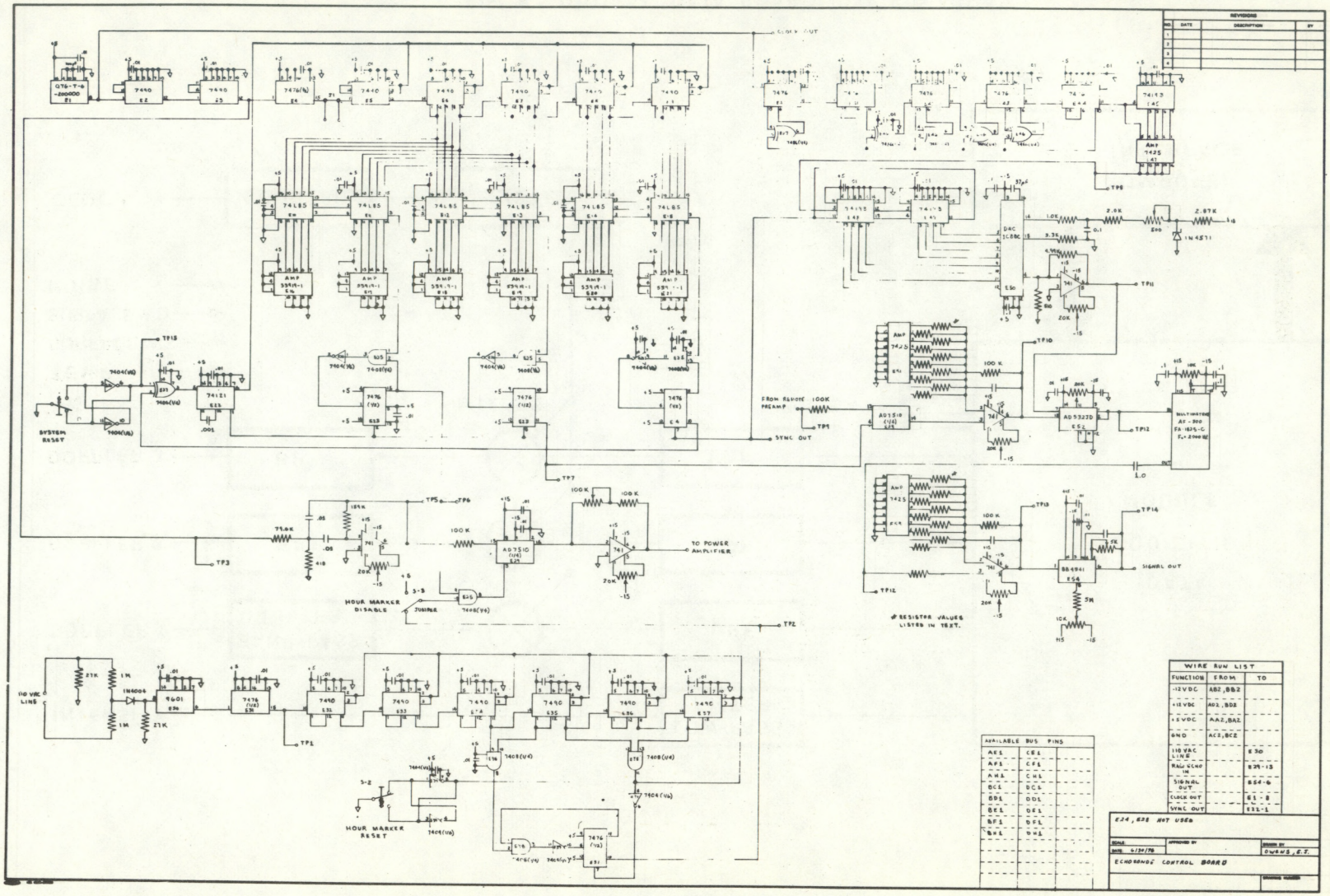

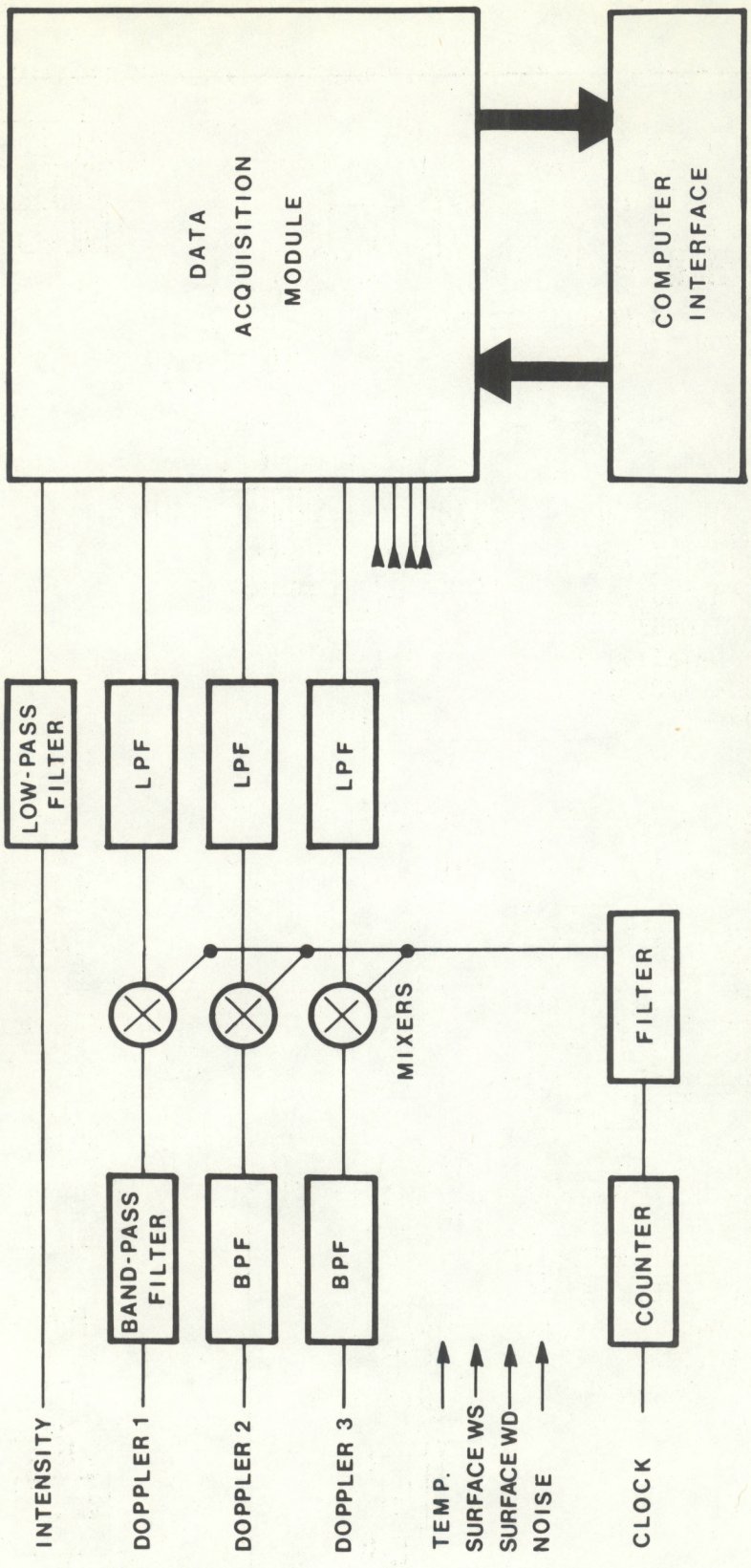

Fig. B.1 DIGITAL DATA BOARD BLOCK DIAGRAM

APPENDIX C - PLOTTER TEST ROUTINE COMPUTER PROGRAM

```
      PROGRAM ACDAT1(INPUT,OUTPUT=/1500,TAPE1,TAPE2=OUTPUT)
      INTEGER A1(200),A(27)
      DIMENSION IDATA1(125)
      DATA I2/"^E^*"/,I3/"^B^*"/,I4/"^H^*"/,I5/"^I^*"/
      DATA I6/"^N^*"/,I7/"^U^*"/,I8/"^V^*"/,I9/"^T^*"/,I10/"^Y^*"/
      DATA I1/555576505555555555 5B/
      L=767343767343767342 55B
      NREC=0
      IREC=500
      NSAMP=125
      N=0
   20 N=N+1
      NPNT=125
      READ(1,100)(IDATA1(J),J=1,125)
  100 FORMAT(1X,125I1)
      DO 40 J=1,NPNT
      NDATA1=IDATA1(J)+1
      GO TO(1,1,1,2,3,4,6,7,9,10),NDATA1
    1 A1(J)=I1
      GO TO 40
    2 A1(J)=I2
      GO TO 40
    3 A1(J)=I3
      GO TO 40
    4 A1(J)=I4
      GO TO 40
    5 A1(J)=I5
      GO TO 40
    6 A1(J)=I6
      GO TO 40
    7 A1(J)=I7
      GO TO 40
    8 A1(J)=I8
      GO TO 40
    9 A1(J)=I9
      GO TO 40
   10 A1(J)=I9
   40 CONTINUE
      WRITE(2,500)(A1(K),K=1,NPNT),L
  500 FORMAT(1H,125A4,A10)
      IF(N.GE.IREC)GOTO25
      GOTO 20
   25 STOP
      END
```

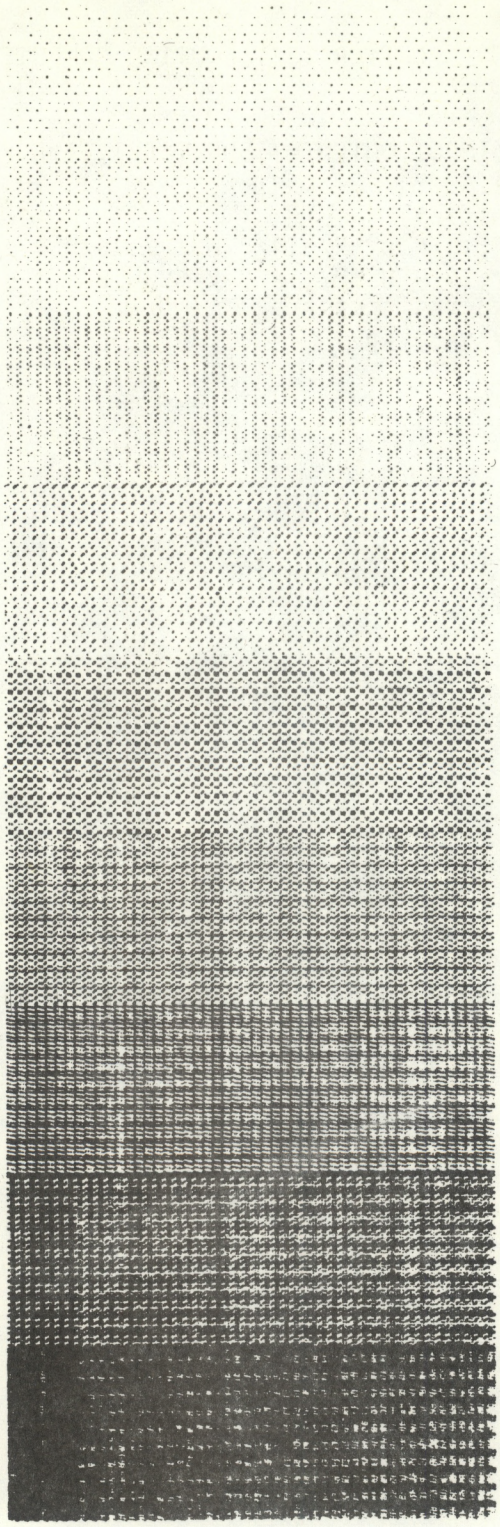

Fig. C.1 Plotter grey shade diagram.

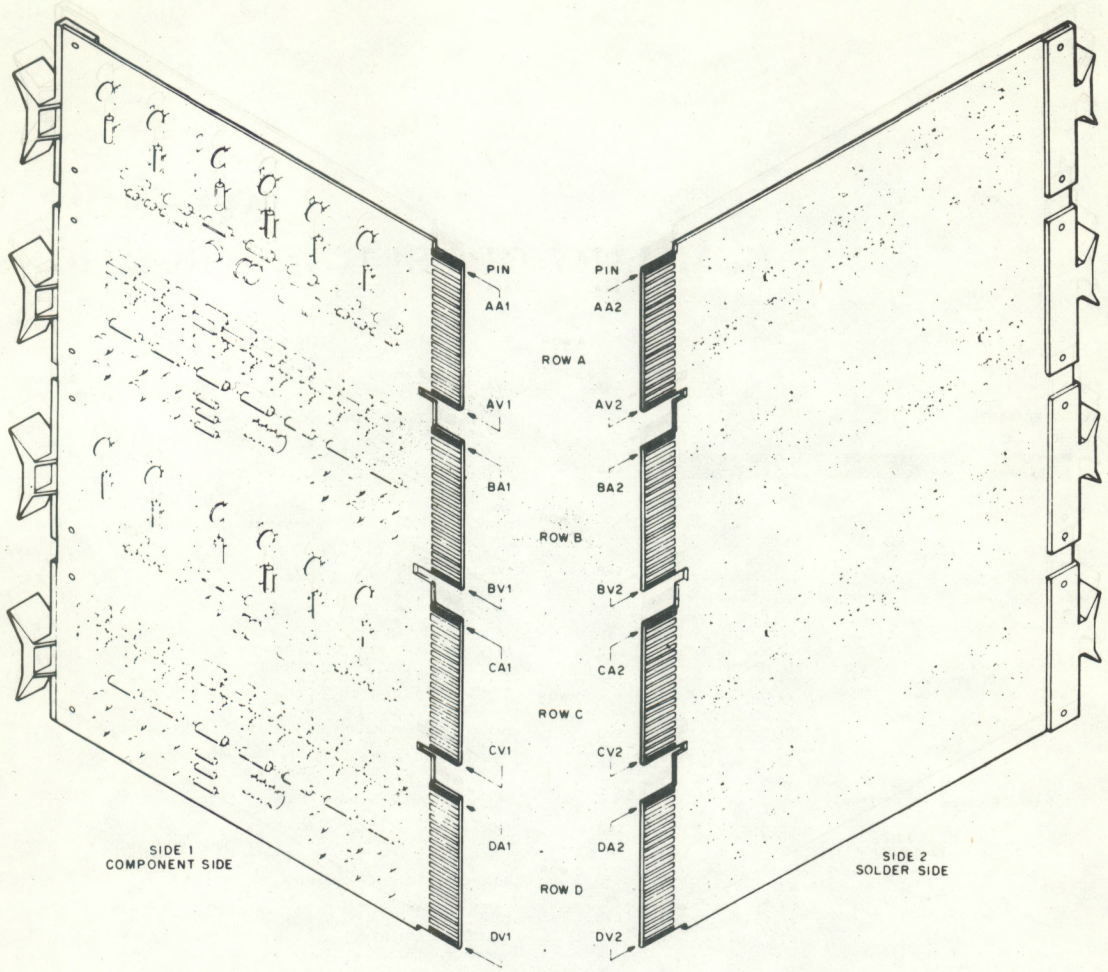

Fig. D.1 Quad module contact finger identification

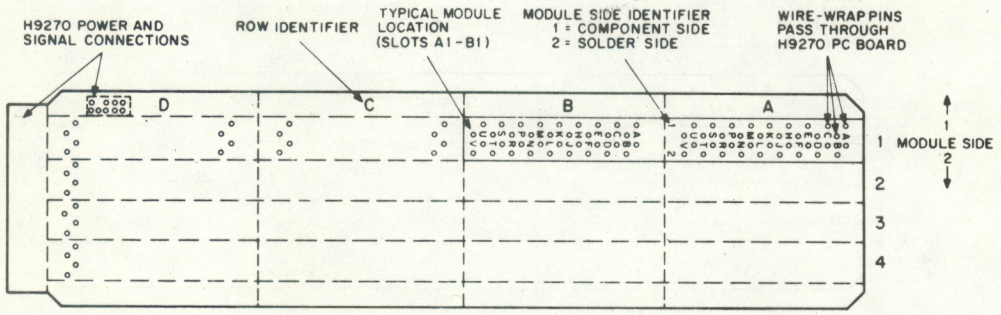

Fig. D.2 LSI-11 Backplane module pin identification

APPENDIX E
SUMMARY OF LSI-11 INSTRUCTIONS

WORD FORMAT

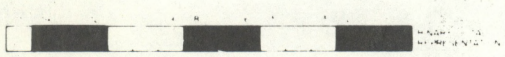

Mode	Name	Symbolic	Description
0	register	R	(R) is operand [ex: R2 = 2]
1	register deferred	(R)	(R) is address
2	auto-increment	(R)+	(R) is adrs, (R) + (1 or 2)
3	auto-incr deferred	@(R)+	(R) is adrs of adrs, (R) + 2
4	auto-decrement	-(R)	(R) - (1 or 2), is adrs
5	auto-decr deferred	@-(R)	(R) - 2, (R) is adrs of adrs
6	index	X(R)	(R) + X is adrs
7	index deferred	@X(R)	(R) + X is adrs of adrs

PROGRAM COUNTER ADDRESSING Reg = 7

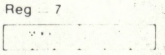

2	immediate	#n operand n follows instr
3	absolute	@#A address A follows instr
6	relative	A instr adrs + 4 + X is adrs
7	relative deferred	@A instr adrs + 4 + X is adrs of adrs

LEGEND

Op Codes

■	0 for word, 1 for byte
SS	source field (6 bits)
DD	destination field (6 bits)
R	gen register (3 bits), 0 to 7
XXX	offset (8 bits), +127 to −128
N	number (3 bits)
NN	number (6 bits)

Operations

( )	contents of
s	contents of source
d	contents of destination
r	contents of register
←	becomes
X	relative address register definition

Boolean

∧	AND
∨	inclusive OR
∀	exclusive OR
¬	NOT

Condition Codes

*	conditionally set, cleared
	not affected
0	cleared
1	set

SINGLE OPERAND: OPR dst

Mnemonic	Op Code	Instruction	dst Result	N	Z	V	C
General							
CLR(B)	■ 050DD	clear	0	0	1	0	0
COM(B)	■ 051DD	complement (1's)	¬d	*	*	0	1
INC(B)	■ 052DD	increment	d + 1	*	*	*	
DEC(B)	■ 053DD	decrement	d − 1	*	*	*	
NEG(B)	■ 054DD	negate (2's compl)	−d	*	*	*	*
TST(B)	■ 057DD	test	d	*	*	0	0
Rotate & Shift							
ROR(B)	■ 060DD	rotate right	→C,d	*	*	*	*
ROL(B)	■ 061DD	rotate left	C,d←	*	*	*	*
ASR(B)	■ 062DD	arith shift right	d/2	*	*	*	*
ASL(B)	■ 063DD	arith shift left	2d	*	*	*	*
SWAB	0003DD	swap bytes		*	*	0	0
Multiple Precision							
ADC(B)	■ 055DD	add carry	d + C	*	*	*	*
SBC(B)	■ 056DD	subtract carry	d − C	*	*	*	*
SXT	0067DD	sign extend	0 or −1		*	0	
Processor Status (PS) Operators							
MFPS	1067DD	move byte from PS	d ← PS	*	*	0	
MTPS	1064SS	move byte to PS	PS ← s	*	*	*	*

DOUBLE OPERAND: OPR src, dst OPR src, R or OPR R, dst

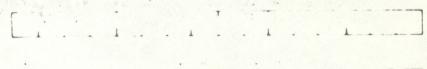

Mnemonic	Op Code	Instruction	Operation	N	Z	V	C
General							
MOV(B)	■ 1SSDD	move	d ← s	*	*	0	
CMP(B)	■ 2SSDD	compare	s − d	*	*	*	*
ADD	06SSDD	add	d ← s + d	*	*	*	*
SUB	16SSDD	subtract	d ← d − s	*	*	*	*
Logical							
BIT(B)	■ 3SSDD	bit test (AND)	s ∧ d	*	*	0	
BIC(B)	■ 4SSDD	bit clear	d ← (¬s) ∧ d	*	*	0	
BIS(B)	■ 5SSDD	bit set (OR)	d ← s ∨ d	*	*	0	
XOR	074RDD	exclusive OR	d ← r ∀ d	*	*	0	

Optional EIS

MUL	070RSS	multiply	r ← r x s	*	*	0	*
DIV	071RSS	divide	r ← r s	*	*	*	*
ASH	072RSS	shift arithmetically		*	*	*	*
ASHC	073RSS	arith shift combined		*	*	*	*

Optional FIS

FADD	07500R	floating add	*	*	0	0
FSUB	07501R	floating subtract	*	*	0	0
FMUL	07502R	floating multiply	*	*	0	0
FDIV	07503R	floating divide	*	*	0	0

BRANCH: B - - location

If condition is satisfied
Branch to location
New PC ← Updated PC − (2 x offset)

adrs of br instr − 2

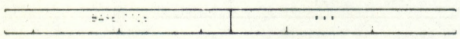

Op Code - Base Code − XXX

Mnemonic	Base Code	Instruction	Branch Condition	
Branches				
BR	000400	branch unconditional	always	
BNE	001000	br if not equal to 0	≠ 0	Z = 0
BEQ	001400	br if equal to 0	= 0	Z = 1
BPL	100000	branch if plus	−	N = 0
BMI	100400	branch if minus	−	N = 1
BVC	102000	br if overflow is clear		V = 0
BVS	102400	br if overflow is set		V = 1
BCC	103000	br if carry is clear		C = 0
BCS	103400	br if carry is set		C = 1
Signed Conditional Branches				
BGE	002000	br if greater or equal to 0	≥0	N ⊕ V = 0
BLT	002400	br if less than 0	<0	N ⊕ V = 1
BGT	003000	br if greater than 0	>0	Z v (N ⊕ V) = 0
BLE	003400	br if less or equal to 0	≤0	Z v (N ⊕ V) = 1
Unsigned Conditional Branches				
BHI	101000	branch if higher	>	C v Z = 0
BLOS	101400	branch if lower or same	≤	C v Z = 1
BHIS	103000	branch if higher or same	≥	C = 0
BLO	103400	branch if lower	<	C = 1

JUMP & SUBROUTINE

Mnemonic	Op Code	Instruction	Notes
JMP	0001DD	jump	PC ← dst
JSR	004RDD	jump to subroutine	use same R
RTS	00020R	return from subroutine	
MARK	0064NN	mark	add in subr return
SOB	077RNN	subtract 1 & br (if ≠ 0)	(R) − 1, then if (R) ≠ 0 PC ← Updated PC − (2 x NN)

TRAP & INTERRUPT:

Mnemonic	Op Code	Instruction	Notes
EMT	104000 to 104377	emulator trap (not for general use)	PC at 30, PS at 32
TRAP	104400 to 104777	trap	PC at 34, PS at 36
BPT	000003	breakpoint trap	PC at 14, PS at 16
IOT	000004	input output trap	PC at 20, PS at 22
RTI	000002	return from interrupt	
RTT	000006	return from interrupt	inhibit T bit trap

MISCELLANEOUS:

Mnemonic	Op Code	Instruction
HALT	000000	halt
WAIT	000001	wait for interrupt
RESET	000005	reset external bus
NOP	000240	no operation

CONDITION CODE OPERATORS:

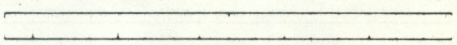

0 = CLEAR SELECTED CONDITION CODE BITS
1 = SET SELECTED CONDITION CODE BITS

Mnemonic	Op Code	Instruction	N	Z	V	C
CLC	000241	clear C	-	-	-	0
CLV	000242	clear V	-	-	0	-
CLZ	000244	clear Z	-	0	-	-
CLN	000250	clear N	0	-	-	-
CCC	000257	clear all cc bits	0	0	0	0
SEC	000261	set C	-	-	-	1
SEV	000262	set V	-	-	1	-
SEZ	000264	set Z	-	1	-	-
SEN	000270	set N	1	-	-	-
SCC	000277	set all cc bits	1	1	1	1

PROCESSOR STATUS WORD

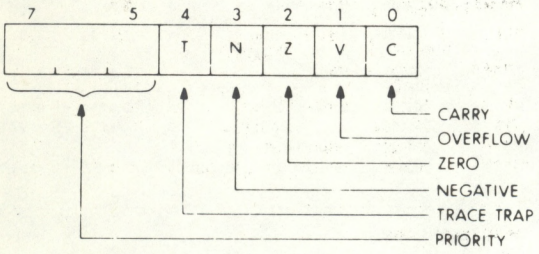

POWERS OF 2

n	2^n	n	2^n
0	1	10	1.024
1	2	11	2.048
2	4	12	4.096
3	8	13	8.192
4	16	14	16.384
5	32	15	32.768
6	64	16	65.536
7	128	17	131.072
8	256	18	262.144
9	512	19	524.288

ABSOLUTE LOADER

Starting Address — 500

Memory Size	
4K	017
8K	037
12K	057
16K	077
20K	117
24K	137
28K	157

BOOTSTRAP LOADER

Address	Contents	Address	Contents
— 744	016 701	— 764	000 002
— 746	000 026	— 766	— 400
— 750	012 702	— 770	005 267
— 752	000 352	— 772	177 756
— 754	005 211	— 774	000 765
— 756	105 711	— 776	177 560 (TTY)
— 760	100 376		
— 762	116 162		

NUMERICAL OP CODE LIST

OP Code	Mnemonic	OP Code	Mnemonic	OP Code	Mnemonic
00 00 00	HALT	00 60 DD	ROR	10 40 00	
00 00 01	WAIT	00 61 DD	ROL	↑	
00 00 02	RTI	00 62 DD	ASR	↓	EMT
00 00 03	BPT	00 63 DD	ASL	10 43 77	
00 00 04	IOT	00 64 NN	MARK		
00 00 05	RESET	00 67 DD	SXT	10 44 00	
00 00 06	RTT			↑	
00 00 07 }	(unused)	00 70 00		↓	TRAP
00 00 77 }		↑	(unused)	10 47 77	
00 01 DD	JMP	↓			
00 02 0R	RTS	00 77 77		10 50 DD	CLRB
				10 51 DD	COMB
		01 SS DD	MOV	10 52 DD	INCB
00 02 10		02 SS DD	CMP	10 53 DD	DECB
↑		03 SS DD	BIT	10 54 DD	NEGB
↓	(reserved)	04 SS DD	BIC	10 55 DD	ADCB
00 02 27		05 SS DD	BIS	10 56 DD	SBCB
		06 SS DD	ADD	10 57 DD	TSTB
00 02 40	NOP				
		07 0R SS	MUL	10 60 DD	RORB
00 02 41		07 1R SS	DIV	10 61 DD	ROLB
↑	cond	07 2R SS	ASH	10 62 DD	ASRB
↓	codes	07 3R SS	ASHC	10 63 DD	ASLB
00 02 77		07 4R DD	XOR	10 64 SS	MTPS
				10 67 DD	MFPS
00 03 DD	SWAB	07 50 0R	FADD		
		07 50 1R	FSUB	11 SS DD	MOVB
00 04 XXX	BR	07 50 2R	FMUL	12 SS DD	CMPB
00 10 XXX	BNE	07 50 3R	FDIV	13 SS DD	BITB
00 14 XXX	BEQ			14 SS DD	BICB
00 20 XXX	BGE	07 50 40		15 SS DD	BISB
00 24 XXX	BLT	↑		16 SS DD	SUB
00 30 XXX	BGT	↓	(unused)		
00 34 XXX	BLE	07 67 77			
00 4R DD	JSR	07 7R NN	SOB		
00 50 DD	CLR	10 00 XXX	BPL		
00 51 DD	COM	10 04 XXX	BMI		
00 52 DD	INC	10 10 XXX	BHI		
00 53 DD	DEC	10 14 XXX	BLOS		
00 54 DD	NEG	10 20 XXX	BVC		
00 55 DD	ADC	10 24 XXX	BVS		
00 56 DD	SBC	10 30 XXX	BCC BHIS		
00 57 DD	TST	10 34 XXX	BCS BLO		

TRAP VECTORS

000	(reserved)	024	Power Fail
004	Time Out & other errors	030	EMT instruction
010	illegal & reserved instr	034	TRAP instruction
014	BPT instruction	244	FIS (optional)
020	IOT instruction		